



TECH BRIEFS

NATIONAL AERONAUTICS AND SPACE ADMINISTRATION

-  **Technology Focus**
-  **Electronics/Computers**
-  **Software**
-  **Materials**
-  **Mechanics/Machinery**
-  **Manufacturing**
-  **Bio-Medical**
-  **Physical Sciences**
-  **Information Sciences**
-  **Books and Reports**

INTRODUCTION

Tech Briefs are short announcements of innovations originating from research and development activities of the National Aeronautics and Space Administration. They emphasize information considered likely to be transferable across industrial, regional, or disciplinary lines and are issued to encourage commercial application.

Availability of NASA Tech Briefs and TSPs

Requests for individual Tech Briefs or for Technical Support Packages (TSPs) announced herein should be addressed to

National Technology Transfer Center

Telephone No. (800) 678-6882 or via World Wide Web at www2.nttc.edu/leads/

Please reference the control numbers appearing at the end of each Tech Brief. Information on NASA's Innovative Partnerships Program (IPP), its documents, and services is also available at the same facility or on the World Wide Web at <http://ipp.nasa.gov>.

Innovative Partnerships Offices are located at NASA field centers to provide technology-transfer access to industrial users. Inquiries can be made by contacting NASA field centers listed below.

NASA Field Centers and Program Offices

Ames Research Center

Lisa L. Lockyer
(650) 604-1754
lisa.l.lockyer@nasa.gov

Dryden Flight Research Center

Gregory Poteat
(661) 276-3872
greg.poteat@dfrc.nasa.gov

Glenn Research Center

Kathy Needham
(216) 433-2802
kathleen.k.needham@nasa.gov

Goddard Space Flight Center

Nona Cheeks
(301) 286-5810
nona.k.cheeks@nasa.gov

Jet Propulsion Laboratory

Ken Wolfenbarger
(818) 354-3821
james.k.wolfenbarger@jpl.nasa.gov

Johnson Space Center

Michele Brekke
(281) 483-4614
michele.a.brekke@nasa.gov

Kennedy Space Center

David R. Makufka
(321) 867-6227
david.r.makufka@nasa.gov

Langley Research Center

Martin Waszak
(757) 864-4015
martin.r.waszak@nasa.gov

Marshall Space Flight Center

Jim Dowdy
(256) 544-7604
jim.dowdy@msfc.nasa.gov

Stennis Space Center

John Bailey
(228) 688-1660
john.w.bailey@nasa.gov

Carl Ray, Program Executive

Small Business Innovation
Research (SBIR) & Small
Business Technology
Transfer (STTR) Programs
(202) 358-4652
carl.g.ray@nasa.gov

Doug Comstock, Director

Innovative Partnerships
Program Office
(202) 358-2560
doug.comstock@nasa.gov



TECH BRIEFS

NATIONAL AERONAUTICS AND SPACE ADMINISTRATION



5 Technology Focus: Sensors

- 5 Induction Charge Detector With Multiple Sensing Stages
- 6 Generic Helicopter-Based Testbed for Surface Terrain Imaging Sensors
- 7 Robot Electronics Architecture
- 7 Optimized Geometry for Superconducting Sensing Coils
- 8 Sensing a Changing Chemical Mixture Using an Electronic Nose



9 Electronics/Computers

- 9 Inertial Orientation Trackers With Drift Compensation
- 10 Microstrip Yagi Antenna With Dual Aperture-Coupled Feed
- 11 Patterned Ferroelectric Films for Tunable Microwave Devices
- 12 Micron-Accurate Laser Fresnel-Diffraction Ranging System
- 13 Efficient G⁴FET-Based Logic Circuits
- 14 Web-Enabled Optoelectronic Particle-Fallout Monitor



15 Materials

- 15 SiO₂/TiO₂ Composite for Removing Hg From Combustion Exhaust
- 16 Lightweight Tanks for Storing Liquefied Natural Gas
- 16 Hybrid Wound Filaments for Greater Resistance to Impacts
- 17 Making High-Tensile-Strength Amalgam Components
- 17 Bonding by Hydroxide-Catalyzed Hydration and Dehydration



19 Mechanics/Machinery

- 19 Balanced Flow Meters Without Moving Parts

- 20 Deflection-Compensating Beam for Use Inside a Cylinder
- 20 Four-Point-Latching Microactuator
- 22 Curved Piezoelectric Actuators for Stretching Optical Fibers
- 23 Tunable Optical Assembly With Vibration Dampening
- 23 Passive Porous Treatment for Reducing Flap Side-Edge Noise
- 24 Cylindrical Piezoelectric Fiber Composite Actuators



27 Manufacturing & Prototyping

- 27 Patterning of Indium Tin Oxide Films
- 27 Gimballed Shoulders for Friction Stir Welding



29 Physical Sciences

- 29 Improved Thermal Modulator for Gas Chromatography
- 30 Nuclear-Spin Gyroscope Based on an Atomic Co-Magnetometer
- 31 Utilizing Ion-Mobility Data To Estimate Molecular Masses
- 32 Optical Displacement Sensor for Sub-Hertz Applications
- 32 Polarization/Spatial Combining of Laser-Diode Pump Beams
- 33 Spatial Combining of Laser-Diode Beams for Pumping an NPRO



35 Information Sciences

- 35 Algorithm Optimally Orders Forward-Chaining Inference Rules
- 35 Project Integration Architecture



37 Books & Reports

- 37 High Power Amplifier and Power Supply
- 37 Estimating Mixing Heights Using Microwave Temperature Profiler
- 37 Multiple-Cone Sunshade for a Spaceborne Telescope

This document was prepared under the sponsorship of the National Aeronautics and Space Administration. Neither the United States Government nor any person acting on behalf of the United States Government assumes any liability resulting from the use of the information contained in this document, or warrants that such use will be free from privately owned rights.



Induction Charge Detector With Multiple Sensing Stages

Standard errors and detection limits are reduced by use of multiple stages.

NASA's Jet Propulsion Laboratory, Pasadena, California

An induction charge detector with multiple sensing stages has been conceived for use in characterizing sprayed droplets, dust particles, large ionized molecules, and the like. Like related prior single-stage devices, each stage yields a measurement of the electric charge and the time of flight of the particle. In effect, an n -stage sensor yields n independent sets of such measurements from the same particle. The benefit of doing this is to increase the effective signal-to-noise ratio and thereby lower the charge-detection limit and the standard error of the charge measurement.

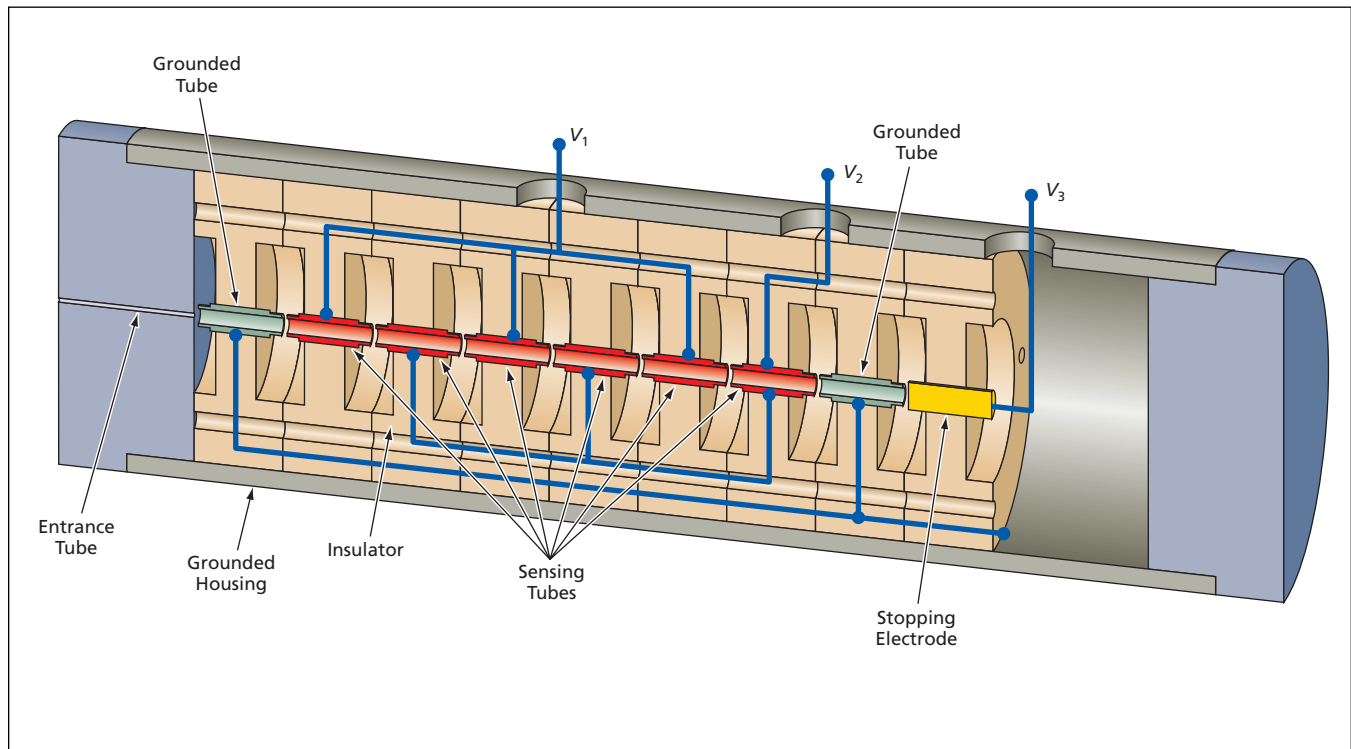
The sensor includes a set of collinear, equal-diameter, electrically conductive cylindrical tubes (sensing tubes) aligned with the path of incoming particles. The entrance to the sensor is a narrower tube that limits the number of entering particles (ideally to one at a time) and ensures that their trajectories remain close

to the cylindrical axis. As a charged particle enters each sensing tube, it induces a charge on the tube nearly equal to its own. Each sensing tube is connected to an operational-amplifier circuit that senses the electric potential associated with the induced charge. The charge of the particle can be calculated from this electric potential and the capacitance of the tube. If the measurement is performed in a vacuum and the particle were accelerated by the use of a known voltage before it entered the sensor, then from (1) the time of flight of the particle as determined from durations of voltage peaks from two consecutive sensing tubes and (2) the known axial distance traversed by the particle, one can calculate the charge-to-mass ratio of the particle. Then from the charge-to-mass ratio and the measured charge, one can calculate the mass of the particle.

The principle of operation of the induction charge detector with multiple

sensing stages is best described by reference to the figure, which shows a cutaway drawing of a three-stage prototype. In this case, there are eight electrically conductive tubes. The first and eighth tubes are electrically grounded. The second through seventh tubes are the sensing tubes; they are held in place by electrically insulating supports and are connected to operational amplifiers for measurement of the potentials as described in the next paragraph. Following the eighth tube is a final stopping electrode, which collects the charged particle and is connected to another operational amplifier for measurement of the potential associated with the charge. An electrically grounded housing surrounds all of the aforementioned parts.

The second, fourth, and sixth sensing tubes constitute a three-stage sensing electrode. They are electrically connected to each other, the potential on them is denoted V_1 , and they are con-



Six of the Eight Electrically Conductive Tubes (the sensing tubes) are connected to operational amplifiers, arranged in successive pairs for measurement of V_1 - V_2 peaks induced by a passing charged particle.

nected to the input terminal of an operational amplifier. Similarly, the third, fifth, and seventh sensing tubes constitute another three-stage sensing electrode; they are electrically connected to each other, the potential on them is denoted V_2 , and they are connected to the input terminal of another operational amplifier. The potential on the stopping electrode is denoted V_3 , and this electrode is connected to the input terminal of a third operational amplifier. In operation, V_1 - V_2 is measured as a function of time. As a particle travels along the sequence of six tubes, it induces a three-cycle V_1 - V_2 waveform, each cycle representing the reading from one of the three sensor stages. The charge measurement for each stage can be calcu-

lated as the product of (1) the magnitude of the corresponding V_1 - V_2 peak reading and (2) a calibration factor obtained from the V_3 reading.

If the readings are analyzed in the time domain, then the use of n detector stages reduces the standard error of the charge measurement, which is proportional to $n^{-1/2}$. On the other hand, because of its periodicity, the waveform lends itself naturally to analysis in the frequency domain. The minimum detectable charge can be reduced, in the case of frequency-domain analysis, by increasing the number of available waveform cycles and, hence, by increasing the number of stages.

However, increasing the number of stages without limit does not reduce the

frequency-domain minimum detectable charge without limit and does not reduce the time-domain standard error without limit. The reason for this is that increasing the number of stages increases the sensor input capacitance, thereby reducing sensitivity. This obstacle can be overcome by the use of a multiblock sensor assembly, recording the output of each block independently. Each block would comprise a multiple-stage sensor as described above, except that the number of stages (not necessarily 3) would be chosen, in conjunction with other design parameters, to optimize performance.

This work was done by Manuel Gamero-Castaño of Caltech for NASA's Jet Propulsion Laboratory. For more information contact iaoffice@jpl.nasa.gov. NPO-44736

Generic Helicopter-Based Testbed for Surface Terrain Imaging Sensors

This flexible field test system is designed for sensors that require an aerial test platform.

NASA's Jet Propulsion Laboratory, Pasadena, California

To be certain that a candidate sensor system will perform as expected during missions, we have developed a field test system and have executed test flights with a helicopter-mounted sensor platform over desert terrains, which simulate Lunar features. A key advantage to this approach is that different sensors can be tested and characterized in an environment relevant to the flight needs prior to flight. Testing the various sensors required the development of a field test system, including an instrument to validate the "truth" of the sensor system under test. The field test system was designed to be flexible enough to cover the test needs of many sensors (lidar, radar, cameras) that require an aerial test platform, including helicopters, airplanes, unmanned aerial vehicles (UAV), or balloons. To validate the performance of the sensor under test, the dynamics of the test platform must be known with sufficient accuracy to provide accurate models for input into algorithm development. The test system provides support equipment to measure the dynamics of the field test sensor platform, and allow computation of the "truth" position, velocity, attitude, and time.

The first test of the field test system provided verification and truth measurements to the LAND (Lunar Access

Navigation Device) laser radar, which enable the comparison of the instrument data versus "ground truth" measurement. The instrumentation includes a GPS (Global Positioning System) receiver, Inertial Measurement Unit (IMU), two visible cameras, a support video camera, and a data collection and time-tagging system. These instruments are mounted on a gyro-stabilized gimbal platform attached to the nose of a helicopter. The gimbal is covered by a dome to reduce the amount of aerodynamic drag on the helicopter, with an observation window, which allows the instruments to view the ground below. The gyro-stabilized platform operates in both "nadir" mode, with the sensors pointed with a fixed angle to the ground, and in "geo" mode, in which the gimbal is directed to a fixed GPS location on the ground. The modes can be changed by a ground team via radio remote control during flight.

During an actual flight test, the flight verification equipment includes three computers for collecting data and controlling instruments. The first laptop performs the timing and synchronization of all equipment and logs IMU and GPS data, as well as recording the synchronization pulses from the LAND system (this could potentially be any other sensor) and provides the image

trigger pulses to the cameras. These data are fed to the laptop through an interface box into a PCMCIA (Personal Computer Memory Card International Association) interface card, which contains a field-programmable gate array (FPGA). This part of the system builds on heritage from a field test done for the Descent Imager Motion Estimation System (DIMES) project for the Mars Exploration Rover project in 2002.

A second laptop contains a GUI to control the LAND system. Commands are sent through an Ethernet interface to the LAND computer using TCP/IP protocol (Transmission Control Protocol/Internet Protocol). These commands control the start/stop of the laser radar, and the number of lidar frames to gather for a single run, as well as also giving estimated altitude measurements to the LAND system. A third computer acts as a digital video recorder (DVR) for acquiring and time-tagging images taken by the two visible cameras.

Summarizing, the architecture includes the use of guidance and control instruments, data collection equipment, flight and ground procedures, ground fixed position reference targets, and data analysis tools. The test system also provides the processing of the collected instrument data, and includes image motion compensation

using the attitude/position instrumentation. This resulted in providing test and validation of an imaging lidar, and has the capability to test other types of surface terrain imaging sensors during aerial field tests. This task thus provides data and truth measurements to

algorithms for a variety of applications including precision Lunar landing algorithm development.

This work was done by James Alexander, Hannah Goldberg, James Montgomery, Gary Spiers, Carl Liebe, Andrew Johnson, Konstantin Gromov, Edward Konefat, Raymond

Lam, and Patrick Meras of Caltech for NASA's Jet Propulsion Laboratory.

The software used in this innovation is available for commercial licensing. Please contact Karina of the California Institute of Technology at (626) 395-2322. Refer to NPO-44581.

Robot Electronics Architecture

Key features are modularity and expandability.

NASA's Jet Propulsion Laboratory, Pasadena, California

An electronics architecture has been developed to enable the rapid construction and testing of prototypes of robotic systems. This architecture is designed to be a research vehicle of great stability, reliability, and versatility. A system according to this architecture can easily be reconfigured (including expanded or contracted) to satisfy a variety of needs with respect to input, output, processing of data, sensing, actuation, and power.

The architecture affords a variety of expandable input/output options that enable ready integration of instruments, actuators, sensors, and other devices as independent modular units. The separation of different electrical functions onto independent circuit boards facilitates the development of corresponding simple and modular software interfaces. As a result, both hardware and software can be made to expand or contract in modular fashion while expending a minimum of time and effort.

To ensure modularity and reconfigurability, the architecture incorporates the PC/104 standard [an industry standard for compact, stackable modules that are fully compatible (in architecture, hardware, and software) with personal-computer

data- and power-bus circuitry]. This feature also enables minimization of development costs through selection of off-the-shelf PC/104 components whenever possible.

Particularly notable is a capability for modular expansion to enable a single central processing unit (CPU) to supervise the simultaneous operation of a practically unlimited number of actuators. For this purpose, the architecture provides for each actuator a modular real-time control subsystem, independent of other such subsystems. The subsystem contains dedicated electronic hardware that drives the actuator to execute continuously updated arbitrary motions. The architecture includes a provision for control feedback in the form of outputs from any or all of a variety of sensors. Any or all actuators can be run independently and motions updated instantly, without reference to any prior motion profile.

A custom actuator-driver circuit board has been developed for this architecture to satisfy some power and mass constraints pertaining to a specific application. This board is capable of driving 12 motors simultaneously under computer control and is built on a standard

PC/104 footprint.

The architecture includes several user- and system-friendly features: Two independent inputs for panic buttons or watchdog functions enable manual, computer, or watchdog disablement of any or all boards, without affecting the computer. An independent circuit holds all actuators inactive until the computer sends an enabling signal. A single switch overrides all functions to enable manual control. Lights, test points, and outputs enable both the user and the computer to independently monitor the state of the board and internal circuit functions.

This work was done by Michael Garrett, Lee Magnone, Hrand Aghazarian, Eric Baumgartner, and Brett Kennedy of Caltech for NASA's Jet Propulsion Laboratory.

In accordance with Public Law 96-517, the contractor has elected to retain title to this invention. Inquiries concerning rights for its commercial use should be addressed to:

Innovative Technology Assets Management, JPL, Mail Stop 202-233, 4800 Oak Grove Drive, Pasadena, CA 91109-8099, (818) 354-2240, E-mail: iaoffice@jpl.nasa.gov.

Refer to NPO-41784, volume and number of this NASA Tech Briefs issue, and the page number.

Optimized Geometry for Superconducting Sensing Coils

Design would minimize measurement time in magnetic resonance imaging.

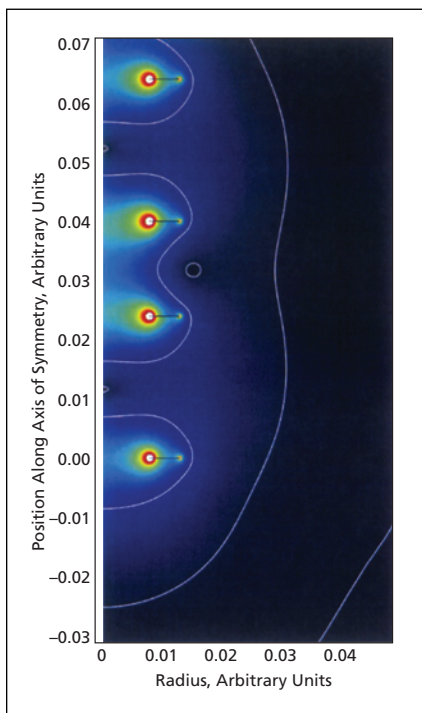
NASA's Jet Propulsion Laboratory, Pasadena, California

An optimized geometry has been proposed for superconducting sensing coils that are used in conjunction with superconducting quantum interference devices (SQUIDS) in magnetic resonance imaging (MRI), magnetoencephalography (MEG), and related applications in which magnetic fields of small dipoles are detected. In designing a coil of this type, as in designing other sensing coils, one seeks

to maximize the sensitivity of the detector of which the coil is a part, subject to geometric constraints arising from the proximity of other required equipment. In MRI or MEG, the main benefit of maximizing the sensitivity would be to enable minimization of measurement time.

In general, to maximize the sensitivity of a detector based on a sensing coil coupled with a SQUID sensor, it is necessary

to maximize the magnetic flux enclosed by the sensing coil while minimizing the self-inductance of this coil. Simply making the coil larger may increase its self-inductance and does not necessarily increase sensitivity because it also effectively increases the distance from the sample that contains the source of the signal that one seeks to detect. Additional constraints on the size and shape of the coil and on the



This False-Color Plot represents half-meridional-plane contours of the magnetic field that would be generated by driving current through the four washerlike turns of an optimized second-order gradiometer sensing coil of the type described in the text.

distance from the sample arise from the fact that the sample is at room temperature but the coil and the SQUID sensor must be enclosed within a cryogenic shield to maintain superconductivity.

One element of an approach to increasing sensitivity without appreciably increasing size is to increase the number of turns, subject to the requirement to maintain an impedance match with the SQUID sensor. On the other hand, simply increasing the number of turns also increases the self-inductance. One way to effect a substantial reduction in inductance without reducing the number of turns is to make the coil of a thicker wire and/or to shape the wire to other than a commonly available circular or square cross section, as described in “Improved Sensing Coils for SQUIDS” (NPO-44397), NASA Tech Briefs, Vol. 31, No. 10 (October, 2007), page 26. On the other hand, the allowable increase in size and change in shape of the wire is limited by the above-mentioned geometric constraints pertaining to enclosure in the cryogenic shield and distance from the sample.

Taking all of the aforementioned considerations into account, it was found that for both SQUID MRI and SQUID MEG, the optimum or nearly optimum coil geometry

would be realized by constructing each turn of the coil in the form of a thin washer. Moreover, in the case of a four-turn coil in a second-order gradiometer arrangement (see figure), it would be beneficial to axially separate the two middle turns in order to further reduce the self-inductance. It has been estimated that for an MRI coil designed according to the present optimized geometry, the increase in sensitivity over that of the corresponding conventional wire-wound coil would make it possible to reduce measurement time by a half.

This work was done by Byeong Ho Eom, Konstantin Penanen, and Inseob Hahn of Caltech for NASA’s Jet Propulsion Laboratory. Further information is contained in a TSP (see page 1).

In accordance with Public Law 96-517, the contractor has elected to retain title to this invention. Inquiries concerning rights for its commercial use should be addressed to:

*Innovative Technology Assets Management
JPL*

*Mail Stop 202-233
4800 Oak Grove Drive
Pasadena, CA 91109-8099*

E-mail: iaoffice@jpl.nasa.gov

Refer to NPO-44629, volume and number of this NASA Tech Briefs issue, and the page number.

Sensing a Changing Chemical Mixture Using an Electronic Nose ASIC may enable continuous, high-speed monitoring.

NASA’s Jet Propulsion Laboratory, Pasadena, California

A method of using an electronic nose to detect an airborne mixture of known chemical compounds and measure the temporally varying concentrations of the individual compounds is undergoing development. In a typical intended application, the method would be used to monitor the air in an inhabited space (e.g., the interior of a building) for the release of solvents, toxic fumes, and other compounds that are regarded as contaminants. At the present state of development, the method affords a capability for identifying and quantitating one or two compounds that are members of a set of some number (typically of the order of a dozen) known compounds. In principle, the method could be extended to enable monitoring of more than two compounds.

An electronic nose consists of an array of sensors, typically made from polymer-carbon composites, the electrical resistances of which change upon exposure to

a variety of chemicals. By design, each sensor is unique in its responses to these chemicals: some or all of the sensitivities of a given sensor to the various vapors differ from the corresponding sensitivities of other sensors. In general, the responses of the sensors are nonlinear functions of the concentrations of the chemicals. Hence, mathematically, the monitoring problem is to solve the set of time-dependent nonlinear equations for the sensor responses to obtain the time-dependent concentrations of individual compounds.

In the present developmental method, successive approximations of the solution are generated by a learning algorithm based on independent-component analysis (ICA) — an established information-theoretic approach for transforming a vector of observed interdependent signals into a set of signals that are as nearly statistically independent as possible. The algorithm can be characterized as being

equivalent to a computational architecture known in the art as a space-invariant ICA architecture. In principle, this architecture is amenable to implementation in an application-specific integrated circuit (ASIC). The anticipated future development of such an ASIC would make it possible to construct a miniature, high-speed, low-power electronic-nose sensor system for continuous monitoring.

This work was done by Tuan Duong and Margaret Ryan of Caltech for NASA’s Jet Propulsion Laboratory.

In accordance with Public Law 96-517, the contractor has elected to retain title to this invention. Inquiries concerning rights for its commercial use should be addressed to:

*Innovative Technology Assets Management,
JPL, Mail Stop 202-233, 4800 Oak Grove Drive, Pasadena, CA 91109-8099, (818) 354-2240, E-mail: iaoffice@jpl.nasa.gov.*

Refer to NPO-42213, volume and number of this NASA Tech Briefs issue, and the page number.



Inertial Orientation Trackers With Drift Compensation

Invention could enable the paralyzed to control machines via head motions.

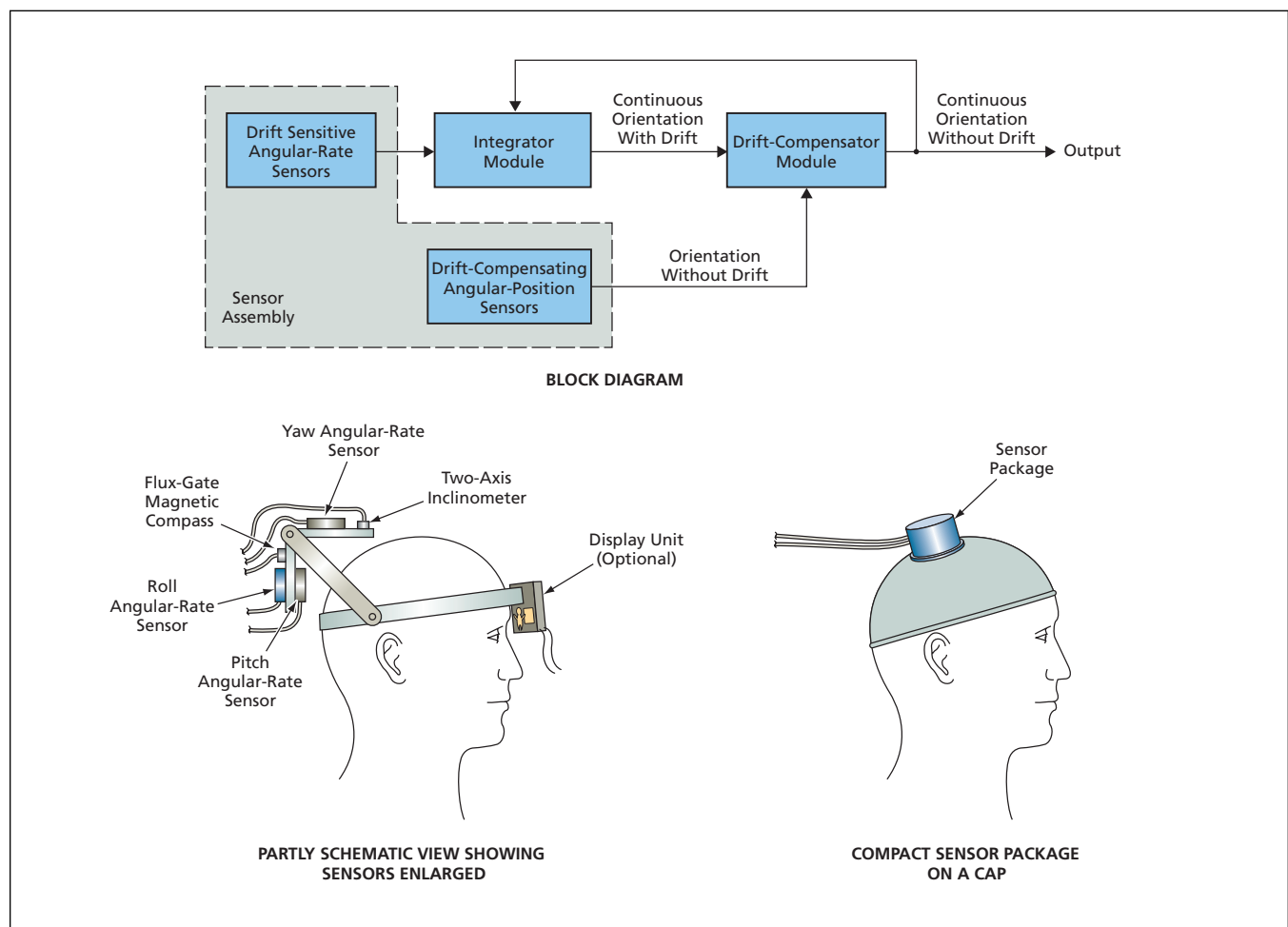
Ames Research Center, Moffett Field, California

A class of inertial-sensor systems with drift compensation has been invented for use in measuring the orientations of human heads (and perhaps other, similarly sized objects). These systems can be designed to overcome some of the limitations of prior orientation-measuring systems that are based, variously, on magnetic, optical, mechanical-linkage, and acoustical principles. The orientation signals generated by the systems of this invention could be used for diverse purposes, including controlling head-orientation-dependent "virtual reality" visual displays or enabling persons whose limbs are paralyzed to control machinery by means of head motions.

The inventive concept admits to variations too numerous to describe here, making it necessary to limit this description to a typical system, the selected aspects of which are illustrated in the figure. A set of sensors is mounted on a bracket on a band or a cap that gently but firmly grips the wearer's head to be tracked. Among the sensors are three drift-sensitive rotation-rate sensors (e.g., integrated-circuit angular-rate-measuring gyroscopes), which put out DC voltages nominally proportional to the rates of rotation about their sensory axes. These sensors are mounted in mutually orthogonal orientations for measuring rates of rotation about the roll, pitch, and

yaw axes of the wearer's head.

The outputs of these rate sensors are conditioned and digitized, and the resulting data are fed to an integrator module implemented in software in a digital computer. In the integrator module, the angular-rate signals are jointly integrated by any of several established methods to obtain a set of angles that represent approximately the orientation of the head in an external, inertial coordinate system. Because some drift is always present as a component of an angular position computed by integrating the outputs of angular-rate sensors, the orientation signal is processed further in a drift-compensator software module.



A **Sensor Assembly** contains angular-rate sensors, a two-axis inclinometer, and a magnetic compass, shown in enlarged, partially schematic form in the bottom left view. In a practical application, the assembly would fit in a compact package, as shown in the bottom right view.

Also mounted on the bracket are two drift-compensating angular-position sensors. One of these sensors is typically a two-axis bubble inclinometer that generates voltages proportional to tilts, relative to the gravitational field, about the roll and pitch axes. The other sensor is typically a flux-gate compass that measures the flux densities of the ambient magnetic field along the roll and pitch axes. In principle, the combination of the magnetic-field information and the tilt information can be used to determine the heading in the horizontal plane or, equivalently, the angular position in rotation about the vertical (gravitational) axis.

Because the bubble inclinometer gives accurate readings only when the head is motionless, success in its use depends on the fact that head motion ceases occasion-

ally — on the average, about once every 10 seconds. Within about $\frac{1}{4}$ second after motion has ceased, the fluid in the inclinometer settles to a steady configuration and an inclinometer reading and the associated compass reading are taken at that time. These readings are digitized and fed to the drift-compensator module. The output of this module is a corrected angular-orientation signal, which both (1) constitutes the main orientation-signal output of the system and (2) is fed back to the integrator module for use in coordinate transformations needed to calculate angular velocities and angles.

In a simplistic approach, each set of drift-compensation readings can be used to reset the system, removing all the drift accumulated since the most recent prior reset. However, the abrupt removal of ac-

cumulated drift could jar the user or adversely affect external equipment that utilizes the orientation output. To prevent such jarring, the drift-compensator module removes the drift from the output gradually, rather than all at once. Thus, the drift compensator generates a set of angular-position signals that gradually approach the correct values over time.

This work was done by Eric M. Foxlin of Massachusetts Institute of Technology for Ames Research Center. Further information is contained in a TSP (see page 1).

This invention has been patented by NASA (U.S. Patent No. 6,361,507). Inquiries concerning rights for the commercial use of this invention should be addressed to the Ames Technology Partnerships Division at (650) 604-2954. Refer to ARC-14132-3.

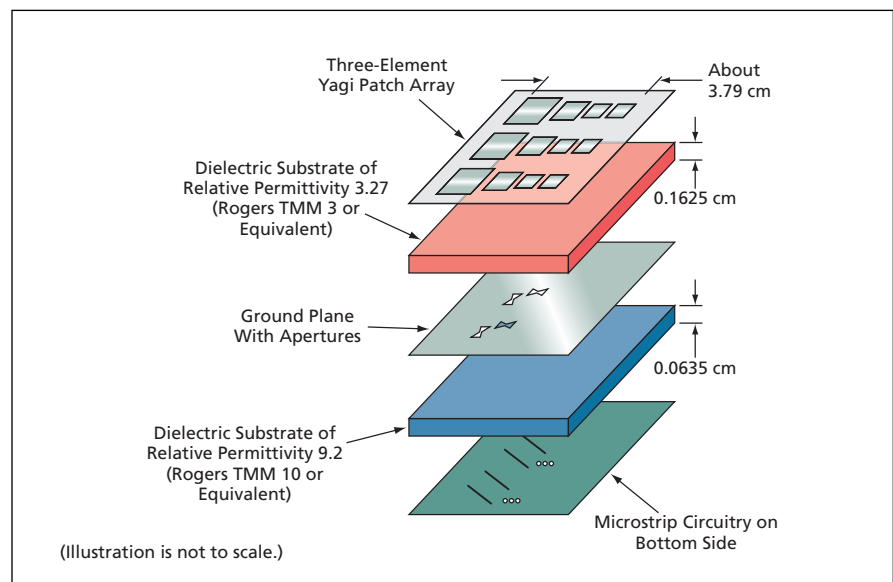
Microstrip Yagi Antenna With Dual Aperture-Coupled Feed

This antenna would have a relatively simple, elegant, low-profile design.

NASA's Jet Propulsion Laboratory, Pasadena, California

antenna is to combine features of a Yagi antenna with those of a microstrip patch to obtain an antenna that can be manufactured at low cost, has a low profile, and radiates a directive beam that, as plotted on an elevation plane perpendicular to the antenna plane, appears tilted away from the broadside. Such antennas are suitable for flush mounting on surfaces of diverse objects, including spacecraft, aircraft, land vehicles, and computers.

The design of the original version of the prior L-band microstrip Yagi antenna utilized a dual coaxial probe feed to generate circularly polarized radiation. (In some other versions of the prior antenna, a single aperture-coupled feed has been used to obtain linear polarization, but this would be of no help in contemplated applications in which circular polarization would be required.) The coaxial feed in the original circular-polarization version introduces electrical and mechanical complexities and difficulties. Electrically, it is difficult to match the impedance of the coaxial cable to that of the antenna because of the parasitics involved in the coaxial through-feed connections. Mechanically, the geometry of the coaxial feed makes it difficult to impart a low profile and predominantly planar character to both the antenna and its feed structure. In contrast, in the proposed X-band microstrip Yagi an-



This **Simplified Exploded View** depicts the main components of the three-element microstrip Yagi antenna featuring dual offset aperture-coupled feed for each patch.

tenna, a dual aperture-coupled feed would be used to obtain circular polarization, simplifying both the electrical and mechanical aspects of design and imparting a predominantly planar character to the overall shape.

Stated somewhat more precisely, what has been proposed is a microstrip antenna comprising an array of three Yagi elements. Each element would include four microstrip-patch Yagi subelements: one re-

flector patch, one driven patch, and two director patches. To obtain circular polarization, each driven patch would be fed by use of a dual offset aperture-coupled feed featuring bow-tie-shaped apertures (see figure). The selection of the dual offset bow-tie aperture geometry is supported by results found in published literature that show that this geometry would enable matching of the impedances of the driven patches to the 50-Ω impedance of the mi-

crostrip feedline while maintaining a desirably large front-to-back lobe ratio.

This work was done by Ronald Pogorzelski and Jaikrishna Venkatesan of Caltech for NASA's Jet Propulsion Laboratory. Further information is contained in a TSP (see page 1).

In accordance with Public Law 96-517, the contractor has elected to retain title to this invention. Inquiries concerning rights for its commercial use should be addressed to:

Innovative Technology Assets Management
JPL
Mail Stop 202-233

4800 Oak Grove Drive
Pasadena, CA 91109-8099
(818) 354-2240
E-mail: iaoffice@jpl.nasa.gov
Refer to NPO-41791, volume and number of this NASA Tech Briefs issue, and the page number.

Patterned Ferroelectric Films for Tunable Microwave Devices

Microwave performance is enhanced by appropriate patterning.

John H. Glenn Research Center, Cleveland, Ohio

Tunable microwave devices based on metal terminals connected by thin ferroelectric films (see Figure 1) can be made to perform better by patterning the films to include suitably dimensioned, positioned, and oriented constrictions. The patterns (see Figure 2) can be formed during fabrication by means of selective etching processes.

The following observations regarding prior ferroelectric-based microwave devices and circuits constitute part of the background and impetus for the present patterning concept:

- The basic principle of design and operation of a ferroelectric-based microwave device calls for a continuous film of ferroelectric material that extends from one metal terminal to another on a low-loss dielectric substrate.
- The performances of conventional ferroelectric-based devices and circuits can be degraded by excessive losses and spurious resonances.
- Designers often seek to obtain linear tuning-versus-bias-voltage profiles. In general, the tuning-versus-bias voltage profile of such a device is difficult to control in the absence of suitable patterning. The desired linear profiles (more specifically, changes in frequency or phase proportional to changes in bias voltage) have not been observed.
- Ferroelectric materials are intrinsically lossy, and losses are especially pronounced in ferroelectric-based narrow-band filters, in which resonant elements must be separated by large distances to obtain the necessary isolation. In a typical prior ferroelectric-based device, the electric field is distributed uniformly across the unpatterned ferroelectric film; hence, if such a film is part of a narrow-band filter, spanning the required large distance, and the loss can be unacceptably high.

• Heretofore, the high permittivities of ferroelectric materials have given rise to large capacitances that have been detrimental to performance at microwave frequencies.

If the width of the ferroelectric film in such a device is reduced at one or more locations, then both the microwave field and any applied DC bias (tuning) electric field become concentrated at

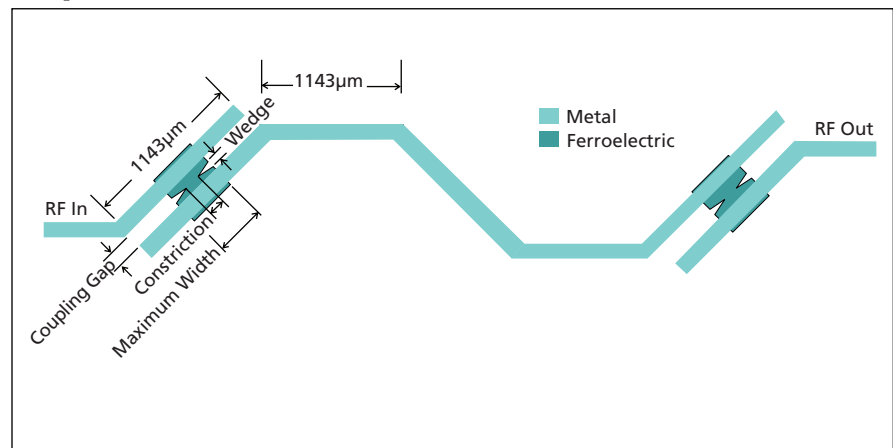


Figure 1. A Tunable Microwave Device is exemplified here as a one-pole microstrip filter with etched ferroelectric layer.

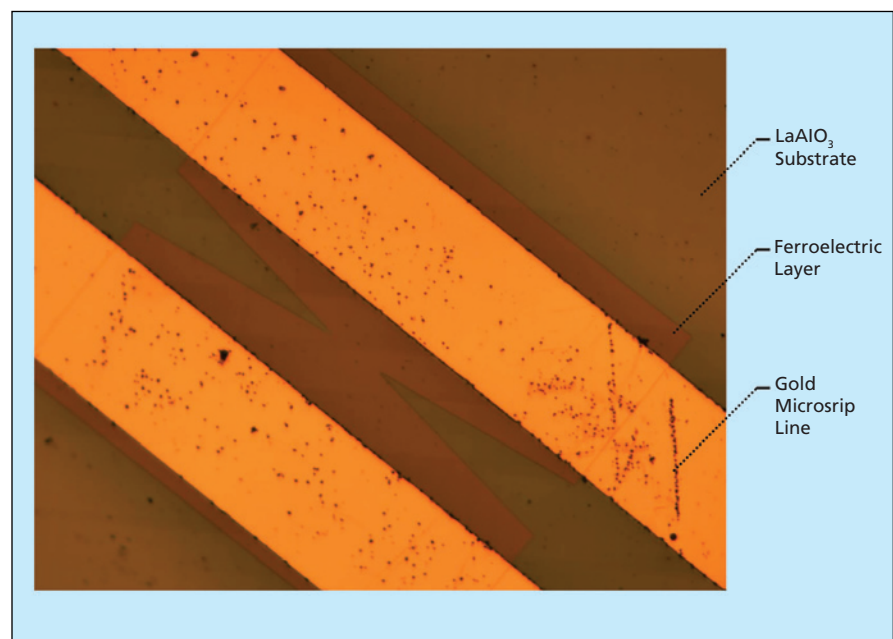


Figure 2. A Coupled Section of the Filter shows etched ferroelectric layer.

those locations. The magnitudes of both the permittivity and the dielectric loss of a ferroelectric material are reduced by application of a DC field. Because the concentration of the DC field in the constriction(s) magnifies the permittivity- and loss-reducing effects of the applied DC voltage, the permittivity and dielectric loss in the constriction(s) are smaller in the constriction(s) than they are in the wider parts of the ferroelectric film. Furthermore, inasmuch as displacement current must flow through either the constriction(s) or the low-loss dielectric substrate, the net effect of the constriction(s) is equivalent to that of incorporating one or more low-loss, low-permittivity region(s) in series with the

high-loss, high-permittivity regions. In a series circuit, the properties of the low-capacitance series element (in this case, the constriction) dominate the overall performance. Concomitantly, the capacitance between the metal terminals is reduced.

By making the capacitance between the metal terminals small but tunable, a constriction increases the upper limit of the frequency range amenable to ferroelectric tuning. The present patterning concept is expected to be most advantageous for devices and circuits that must operate at frequencies from about 4 to about 60 GHz. A constriction can be designed such that the magnitude of the microwave electric field and the effective

width of the region occupied by the microwave electric field become functions of the applied DC electric field, so that tunability is enhanced. It should even be possible to design the constriction to obtain a specific tuning-versus-voltage profile.

This work was done by Félix A. Miranda of Glenn Research Center and Carl H. Mueller of Analex Corp. Further information is contained in a TSP (see page 1).

Inquiries concerning rights for the commercial use of this invention should be addressed to NASA Glenn Research Center, Innovative Partnerships Office, Attn: Steve Fedor, Mail Stop 4-8, 21000 Brookpark Road, Cleveland, Ohio 44135. Refer to LEW-17411.

Micron-Accurate Laser Fresnel-Diffraction Ranging System

This system would exploit the variation of Fresnel diffraction with distance.

Marshall Space Flight Center, Alabama

The figure schematically depicts two versions of an optoelectronic system, undergoing development at the time of reporting the information for this article, that is expected to be capable of measuring a distance between 2 and 10 m with an error of no more than 1 μm . The system would be designed to exploit Fresnel diffraction of a laser beam. In particular, it would be designed to take advantage of the fact that a Fresnel diffraction pattern is ultrasensitive to distance.

In either version, a Fresnel diffraction pattern would be generated by aiming a laser beam at a pinhole, the size of which could be varied. The diffracted laser light would illuminate the object, the distance to which was to be measured. The diffracted laser light reflected from that object would be collected by an optical receiver comprising a telescope equipped with an imaging photodetector array at its focal plane. The resulting Fresnel-diffraction-pattern readout from the array would be digitized and sent to a computer. In principle, the digitized Fresnel diffraction pattern could be compared computationally with a set of known Fresnel diffraction patterns for known distances. Once a match was found, the distance of the observed Fresnel pattern would be determined to within a micron. The range of the system would be limited only by the power of the laser, the maximum laser power toler-

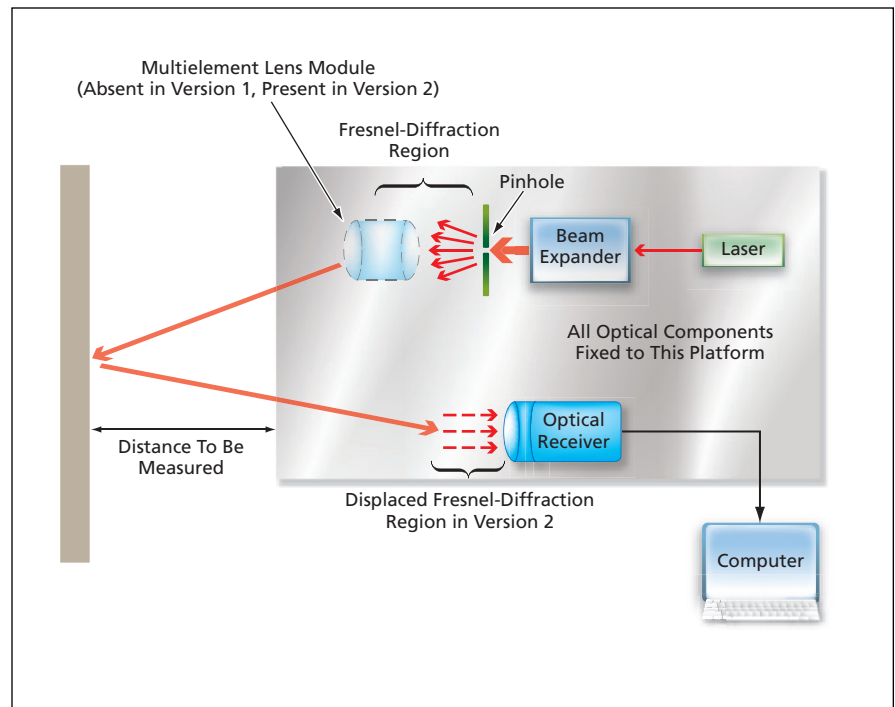
ated by the optical train of the system, and the sensitivity of the photodetector array.

The two versions would differ in the following respects:

- In version 1, the focus of the telescope would be in the Fresnel region, and the telescope would have a small depth of focus. As a consequence, the Fresnel

pattern would be imaged directly onto the photodetector array.

- In version 2, a multielement lens module would displace the Fresnel region from the vicinity of the pinhole to the vicinity of the optical receiver. As the distance to be measured varied, the location of the receiver relative to the displaced Fresnel-diffraction region would



An **Object Would Be Illuminated** with a Fresnel-diffracted laser beam. The distance to the object would be determined by, in effect, inverting the known dependence of the diffraction pattern upon the distance.

vary, thereby causing the Fresnel diffraction pattern on the focal plane to vary. The multielement lens module would also correct for aberrations.

The processing of the digitized Fresnel diffraction pattern in the computer might be accelerated by using only parts of the pattern or even only one small part — the central pixel. As the distance from the pinhole increased, the central pixel would rapidly cycle between maximum and minimum light intensity. This

in itself would not be sufficient to uniquely determine the distance. However, by varying the size of the pinhole or the wavelength of the laser, one could obtain a second cycle of variation of intensity that, in conjunction with the first cycle, could enable a unique determination of distance. Alternatively, for a single wavelength and a single pinhole size, it should suffice to consider the data from only two different key pixels in the Fresnel pattern.

This work was done by David Lehmer, Jonathan Campbell, and Kelly Smith of Marshall Space Flight Center; Duncan Earl and Alvin Sanders of the University of Tennessee; Stephen Allison of Oak Ridge National Laboratory; and Larry Smalley of the University of Alabama in Huntsville.

This invention is owned by NASA, and a patent application has been filed. For further information, contact Sammy Nabors, MSFC Commercialization Assistance Lead, at sammy.a.nabors@nasa.gov. Refer to MFS-31649-1.

Efficient G⁴FET-Based Logic Circuits

Fewer G⁴FETs than conventional transistors would be needed to implement logic functions.

NASA's Jet Propulsion Laboratory, Pasadena, California

A total of 81 optimal logic circuits based on four-gate field-effect transistors (G⁴FETs) have been designed to implement all Boolean functions of up to three variables. The purpose of this development was to lend credence to the expectation that logic circuits based on G⁴FETs could be more efficient (in the sense that they could contain fewer transistors), relative to functionally equivalent logic circuits based on conventional transistors.

The theoretical basis of this development was summarized in "G⁴FETs as Universal and Programmable Logic Gates" (NPO-41698) *NASA Tech Briefs*, Vol. 31, No. 7 (July 2007), page 44. To recapitulate: A G⁴FET is a combination of a junction field-effect transistor (JFET) and a metal oxide/semiconductor field-effect transistor (MOSFET) superimposed in a single

silicon island and can therefore be regarded as two transistors sharing the same body. A G⁴FET can also be regarded as a single device having four gates: two side junction-based gates, a top MOS gate, and a back gate activated by biasing of a silicon-on-insulator substrate. Each of these gates can be used to control the conduction characteristics of the transistor; this possibility creates new options for designing analog, radio-frequency, mixed-signal, and digital circuitry. One such option is to design a G⁴FET to function as a three-input NOT-majority gate, which has been shown to be a universal and programmable logic gate. The universality and programmability could be exploited to design logic circuits containing fewer discrete components than are required for conventional transistor-

based circuits implementing the same logic functions.

Optimal NOT-majority-gate, G⁴FET-based logic-circuit designs were obtained in a comparative study that also included formulation of functionally equivalent logic circuits based on NOR and NAND gates implemented by use of conventional transistors. [NOT gates (inverters) were also included, as needed, in both the G⁴FET- and the NOR- and NAND-based designs.] In the study, the problem of finding the optimal design for each logic function and each transistor type was solved as an integer-programming optimization problem. The table summarizes results obtained in this study for the first four Boolean functions, showing that in most cases, fewer logic gates are needed in the NOT-majority (G⁴FET) implementation than in the NOR- and

Function	NOT-Majority (G ⁴ FET) Implementation		Conventional NOR Implementation		Conventional NAND Implementation	
	Number of NOT-Majority Gates	Number of NOT Gates	Number of NOR Gates	Number of NOT Gates	Number of NAND Gates	Number of NOT Gates
{1,0,0,0,0,0,0,0} = \overline{ABC}	2	1	2	1	4	3
{0,1,0,0,0,0,0,0} = $A\overline{BC}$	2	1	3	1	4	2
{0,0,0,1,0,0,0,0} = $AB\overline{C}$	2	0	2	3	3	2
{0,0,0,0,0,0,0,1} = ABC	2	1	2	4	3	1

Numbers of Logic Gates were calculated for optimal circuits implementing several Boolean functions of the three input variables (A,B,C). Each entry in the "Function" column includes an octuple binary representation of the noted Boolean function, namely {f(0,0,0),f(0,0,1),f(0,1,0),f(0,1,1),f(1,0,0),f(1,0,1),f(1,1,0),f(1,1,1)}.

NAND-based conventional implementations. Considering all 81 non-equivalent Boolean functions included in the study, it was found that in 63 percent of the cases, fewer logic gates (and, hence, fewer transistors) would be needed in the G⁴FET-based implementations.

This work was done by Farrokh Vatan of Caltech for NASA's Jet Propulsion Laboratory. Further information is contained in a TSP (see page 1).

In accordance with Public Law 96-517, the contractor has elected to retain title to this invention. Inquiries concerning rights for its commercial use should be addressed to:

Innovative Technology Assets Management, JPL, Mail Stop 202-233, 4800 Oak Grove Drive, Pasadena, CA 91109-8099, E-mail: iaoffice@jpl.nasa.gov.

Refer to NPO-44407, volume and number of this NASA Tech Briefs issue, and the page number.

Web-Enabled Optoelectronic Particle-Fallout Monitor

A user can interrogate this instrument from a remote location.

John F. Kennedy Space Center, Florida

A Web-enabled optoelectronic particle-fallout monitor has been developed as a prototype of future such instruments that (1) would be installed in multiple locations for which assurance of cleanliness is required and (2) could be interrogated and controlled in nearly real time by multiple remote users. Like prior particle-fallout monitors, this instrument provides a measure of particles that accumulate on a surface as an indication of the quantity of airborne particulate contaminants. The design of this instrument reflects requirements to:

- Reduce the cost and complexity of its optoelectronic sensory subsystem relative to those of prior optoelectronic particle fallout monitors while maintaining or improving capabilities;
- Use existing network and office computers for distributed display and control;
- Derive electric power for the instrument from a computer network, a wall outlet, or a battery;
- Provide for Web-based retrieval and analysis of measurement data and of a file containing such ancillary data as a log of command attempts at remote units; and
- Use the User Datagram Protocol (UDP) for maximum performance and minimal network overhead.

The sensory subsystem of the Web-enabled optoelectronic particle-fallout monitor includes an infrared light-emitting diode (LED) that illuminates a silicon wafer. Highly discriminating photodiodes measure the light scattered at right angles to the illumination. The scattered

light is measured both (1) during illumination by the LED and (2) when the LED is turned off so that only ambient light is present. The ambient infrared scattered-light reading is subtracted from the illumination scattered-light reading to obtain a net scattered-light reading. In principle, the amount of scattering attributable to particles on the wafer, and thus the number of particles on the wafer, is closely related to the ratio between the net scattered-light reading and the LED output, with a correction for temperature that affects the photodiode junction and a small additional correction for ambient light. Photodiode readings of the LED output are taken for eventual use in calculating the ratio, and temperature is measured for eventual use in calculating photodiode junction corrections, but at the present prototype stage of development, the ratio and corrections are not calculated and, instead, the number of particles accumulated on the wafer is estimated as being simply proportional to the net scattered-light reading. Other features of the instrument design include the following:

- The instrument includes a built-in Ethernet/Web server communication subsystem and a microprocessor tied directly to this subsystem.
- A power-over-Ethernet feature provides for the use of one wire for control, data communication, and power supply. This feature is also compatible with battery or wall-outlet power.
- The microprocessor receives commands via the Web and/or the Ethernet, initi-

ates and controls operation of the sensory subsystem, and collects data.

- The instrument communicates with a desktop personal computer that is capable of gathering information from as many as 1,000 instruments like this one. The personal computer, in turn, provides information to a Web server computer for archiving and analysis.
- Photodiode outputs are sampled by 24-bit analog-to-digital converters (ADCs), controlled by the microprocessor, at a repetition rate of 20 Hz. Included within the ADCs are filters that suppress, by more than 80 dB, interfering signal components at the 60-Hz power-line frequency that have been found to be present in photodetector outputs of similar prior instruments. An ADC output exhibits a differential count of >25,000 between the clean and 0.5-percent-obscured wafer conditions. The normal sample-to-sample range is within 32 counts.
- Optionally, the instrument can be set to send an electronic-mail message directly to a designated person when an out-of-bounds condition (e.g., a particle count in excess of a prescribed limit) occurs.
- Integrity of data is ensured by use of both UDP checksums and cyclical redundancy checks.

This work was done by Lewis P. Lineberger of Kennedy Space Center. For further information, contact the Kennedy Innovative Partnerships Program Office at (321) 861-7158. KSC-12984



SiO₂/TiO₂ Composite for Removing Hg From Combustion Exhaust

This material could remove mercury from exhaust streams of coal-burning power plants.

Lyndon B. Johnson Space Center, Houston, Texas

Pellets made of a high-surface-area composite of silica and titania have shown promise as means of removing elemental mercury from flue gases. With further technical development and commercialization, this material could become economically attractive as a more-effective, less-expensive alternative to activated carbons for removing mercury from exhaust streams of coal-burning power plants, which are the sources of more than 90 percent of all anthropogenic airborne mercury.

The silica/titania composite is made from a silica precursor and titania, starting with a sol-gel process in which water, a solvent, and acids are used to promote the hydrolysis and condensation reactions. After gelation, the reaction mixtures are aged, rinsed, and then dried in

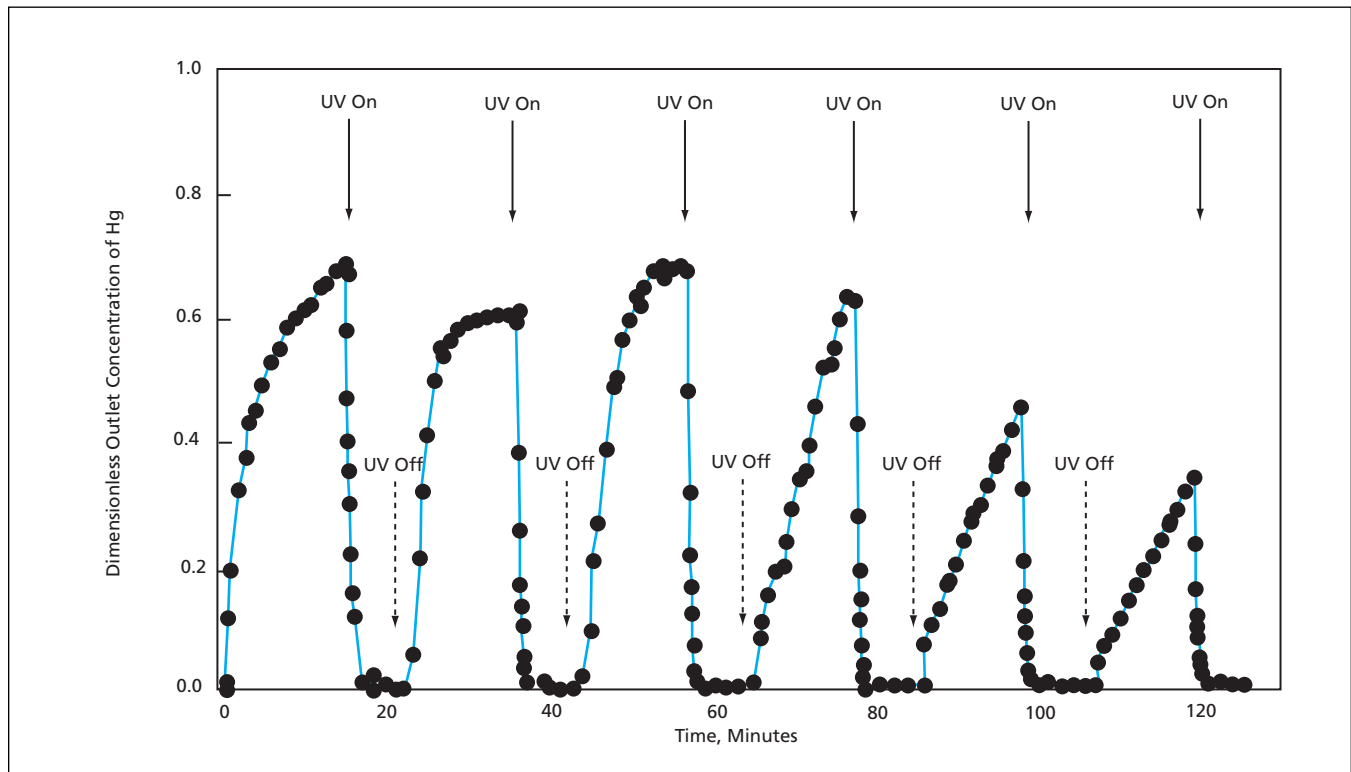
a series of heat treatments. The resulting composite pellets are about 5 mm long and 3 mm wide. Each pellet comprises TiO₂ nanoparticles distributed in a porous SiO₂ matrix. The pores are of the order of 15 nm wide. The pellets are characterized by specific surface area of about 300 m²/g.

This composite material removes elemental mercury from air or a flue-gas mixture through a synergistic combination of (1) adsorption on the surfaces of the composite pellets and (2) photocatalytic oxidation in the presence of ultraviolet light. The mercury oxide remains on the surfaces of the pellets as a solid deposit. From time to time, the mercury oxide can be extracted from the pellets — thereby both regenerating the pellets and making the mercury available for re-

cycling — for example, by rinsing the pellets with acid.

The adsorptive capacity of the composite material is great enough to enable continuous concentration of mercury onto the pellets without continuous use of ultraviolet light (see figure). Intermittent ultraviolet irradiation suffices to ensure oxidation of adsorbed mercury and mercury vapor and to regenerate the adsorbent. The efficiency of removal of Hg can easily be made as high as 99 percent or greater while ultraviolet light is on. Moreover, the photocatalytic oxidation can be said to activate the adsorbent in that it increases the subsequent adsorption capacity in the absence of ultraviolet light.

The mercury-adsorption capacity of the pellets is high although at the 3-mm



The Dimensionless Outlet Concentration of Hg Vapor (that is, the outlet concentration + inlet concentration) was measured in an experiment in which air laden with Hg vapor was pumped through a bed of SiO₂/TiO₂ pellets under periodic exposure to ultraviolet (UV) light. This curve shows that adsorption continued (albeit at a diminishing rate) when the UV light was turned off and that oxidation removed most of the Hg from the outlet stream within about 2 minutes of turning the UV light on.

pellet width, only a thin outer layer is utilized effectively. A TiO₂ loading of 13 weight percent has been found to result in the best removal of Hg, both with and without ultraviolet light. Humidity has been found to impede adsorption, thereby reducing the overall Hg-removal efficiency. An examination of the effects of flow velocity revealed that adsorption

is the rate-limiting step, suggesting a need to improve mass-transfer characteristics to obtain better performance.

This work was done by David Mazyck, Danielle Londeree, Chang-Yu Wu, Kevin Powers, and Erik Pitoniak of the University of Florida for Johnson Space Center.

In accordance with Public Law 96-517, the contractor has elected to retain title to this

invention. Inquiries concerning rights for its commercial use should be addressed to:

*University of Florida,
Environmental Engineering
306 Black Hall
Gainesville, FL 32611*

Refer to MSC-23624, volume and number of this NASA Tech Briefs issue, and the page number.

Lightweight Tanks for Storing Liquefied Natural Gas

These tanks are also relatively inexpensive.

Marshall Space Flight Center, Alabama

Single-walled, jacketed aluminum tanks have been conceived for storing liquefied natural gas (LNG) in LNG-fueled motor vehicles. Heretofore, double-wall steel tanks with vacuum between the inner and outer walls have been used for storing LNG. In comparison with the vacuum-insulated steel tanks, the jacketed aluminum tanks weigh less and can be manufactured at lower cost. Costs of using the jacketed aluminum tanks are further reduced in that there is no need for the vacuum pumps heretofore needed to maintain vacuum in the vacuum-insulated tanks.

The single-walled, jacketed aluminum tanks are members of the class of composite overwrapped pressure vessels; that is, they comprise basically, seamless aluminum tank liners overwrapped in composite (matrix/fiber) materials. On each

such tank, the composite overwrap is further encapsulated in a layer of insulating foam, which, in turn, is coated with a flexible sealant that protects the foam against abrasion, ultraviolet light, and other adverse environmental phenomena.

The innovative tank concept admits to a number of variations. For example, the aluminum tank liner can be a common, commercially available aluminum tank liner that is already certified by the United States Department of Transportation for use at pressure up to 3,000 psi (≈ 20.7 MPa). The composite-material overwrap can be made by winding high-strength-carbon-fiber/poly(phenylene benzo-bisoxazole)-fiber hybrid filaments with an epoxy matrix material. The insulating layer can be made by spraying polyurethane foam, waiting for the foam to cure to rigidity, then machining the

foam to final size and shape. The protective outer layer can be formed by brush application of a ductile epoxy or spray application of a truck-bed-liner material.

Of course, if the tank liner is a pressure vessel as in the example above, then the tank can be used to store a high-pressure gaseous fuel. Moreover, in the case of storage of LNG, the high-pressure capability of the tank helps to conserve stored fuel by reducing the need to vent gas to relieve pressure as heat leaks into the tank, causing slow vaporization of the LNG.

This work was done by Tom DeLay of Marshall Space Flight Center.

This invention is owned by NASA, and a patent application has been filed. For further information, contact Sammy Nabors, MSFC Commercialization Assistance Lead, at sammy.a.nabors@nasa.gov. Refer to MFS-32024-1.

Hybrid Wound Filaments for Greater Resistance to Impacts

PBO fibers are used in addition to high-strength carbon fibers.

Marshall Space Flight Center, Alabama

The immediately preceding article includes an example in which a composite overwrap on a pressure vessel contains wound filaments made of a hybrid of high-strength carbon fibers and poly(phenylene benzobisoxazole) [PBO] fibers. This hybrid material is chosen in an effort to increase the ability of the pressure vessel to resist damage by low-speed impacts (e.g., dropping of tools on the vessel or bumping of the vessel against hard objects during installation and use) without significantly increasing the weight of the vessel. Heretofore, enhancement of the impact resistances of fila-

ment-wound pressure vessels has entailed increases in vessel weight associated, variously, with increases in wall thickness or addition of protective materials.

While the basic concept of hybridizing fibers in filament-wound structures is not new, the use of hybridization to increase resistance to impacts is an innovation, and can be expected to be of interest in the composite-pressure-vessel industry. The precise types and the proportions of the high-strength carbon fibers and the PBO fibers in the hybrid are chosen, along with the filament-winding pattern, to maximize the advan-

tageous effects and minimize the disadvantageous effects of each material. In particular, one seeks to (1) take advantage of the ability of the carbon fibers to resist stress rupture while minimizing their contribution to vulnerability of the vessel to impact damage and (2) take advantage of the toughness of the PBO fibers while minimizing their contribution to vulnerability of the vessel to stress rupture.

Experiments on prototype vessels fabricated according to this concept have shown promising results. At the time of reporting the information for this article, research toward understanding and

optimizing the performances of PBO fibers so as to minimize their contribution to vulnerability of the pressure vessel to stress rupture had yet to be performed.

*This work was done by Thomas K. DeLay of Marshall Space Flight Center and James E. Patterson and Michael A. Olson of HyPer-Comp Engineering, Inc.
This invention is owned by NASA, and a*

patent application has been filed. For further information, contact Sammy Nabors, MSFC Commercialization Assistance Lead, at sammy.a.nabors@nasa.gov. Refer to MFS-31838-1.

Making High-Tensile-Strength Amalgam Components

Instead of spheroids or flakes, wires are used as the solid constituents.

Marshall Space Flight Center, Alabama

Structural components made of amalgams can be made to have tensile strengths much greater than previously known to be possible. Amalgams, perhaps best known for their use in dental fillings, have several useful attributes, including room-temperature fabrication, corrosion resistance, dimensional stability, and high compressive strength. However, the range of applications of amalgams has been limited by their very small tensile strengths. Now, it has been discovered that the tensile strength of an amalgam depends critically on the sizes and shapes of the particles from which it is made and, consequently, the tensile strength can be greatly increased through suitable choice of the particles.

The term “amalgam” generally denotes an alloy of mercury with one or more other metals (e.g., copper or a copper alloy in the case of dental fillings). Amalgams can also be based on gallium, or gallium alloys, which melt near room temperature. An amalgam is formed by a peritectic reaction in a process called “trituration,” in which the solid metal (e.g., copper) in powder form is ground together with the liquid

metal (e.g., gallium). The grinding serves to break the oxide skin on the solid metal particles, enabling wetting of the clean metal surfaces by the liquid metal. The liquid metal reacts with the solid metal to form a new solid that is a composite of the starting solid metal (e.g., Cu) and an intermetallic compound (e.g., CuGa).

Heretofore, the powder particles used to make amalgams have been, variously, in the form of micron-sized spheroids or flakes. The tensile reinforcement contributed by the spheroids and flakes is minimal because fracture paths simply go around these particles. However, if spheroids or flakes are replaced by strands having greater lengths, then tensile reinforcement can be increased significantly. The feasibility of this concept was shown in an experiment in which electrical copper wires, serving as demonstration substitutes for copper powder particles, were triturated with gallium by use of a mortar and pestle and the resulting amalgam was compressed into a mold. The tensile strength of the amalgam specimen was then measured and found to be greater than 10^4 psi (greater than about 69 MPa).

Proceeding forward from this demonstration of feasibility, much remains to be done to optimize the properties of amalgams for various applications through suitable choice of starting constituents and modification of the trituration and molding processes. The choice of wire size and composition is expected to be especially important. Perusal of phase diagrams of metal mixtures could give insight that would enable choices of solid and liquid metal constituents. For example, phase diagrams have revealed that gallium should form amalgams with iron and nickel (as already demonstrated), as well as zirconium, and titanium. Finally, whereas heretofore, only binary alloys have been considered for amalgams, ternary additions to liquid or solid components should be considered as means to impart desired properties to amalgams.

This work was done by Richard Grugel of Marshall Space Flight Center.

This invention is owned by NASA, and a patent application has been filed. For further information, contact Sammy Nabors, MSFC Commercialization Assistance Lead, at sammy.a.nabors@nasa.gov. Refer to MFS-32254-1.

Bonding by Hydroxide-Catalyzed Hydration and Dehydration

Room-temperature process can be varied to suit optical and non-optical applications.

Marshall Space Flight Center, Alabama

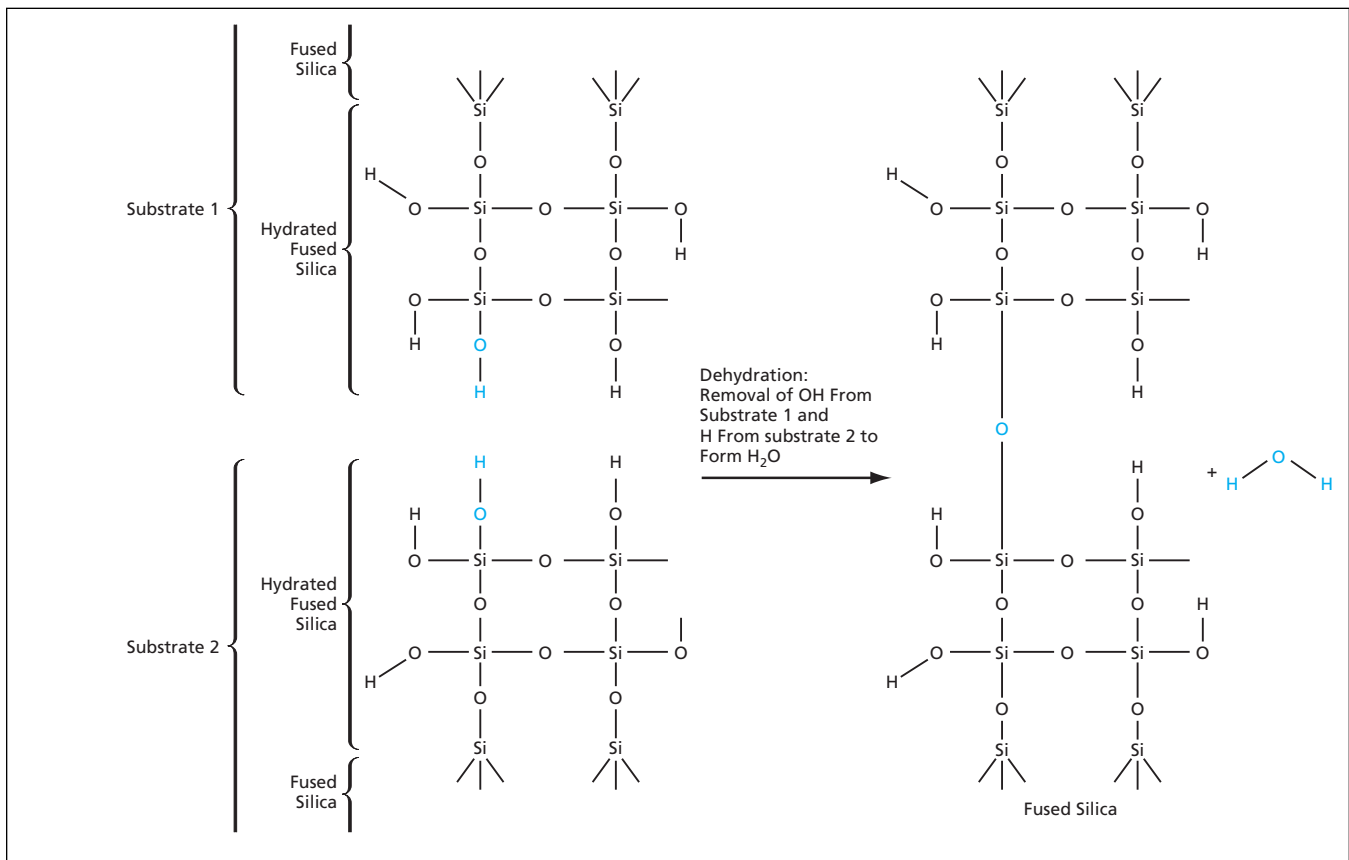
A simple, inexpensive method for bonding solid objects exploits hydroxide-catalyzed hydration and dehydration to form silicatelike networks in thin surface and interfacial layers between the objects. (Silicatelike networks are chemical-bond networks similar to, but looser than, those of bulk silica). The method can be practiced at room temperature or over a wide range of temperatures.

The method was developed especially to enable the formation of precise, reli-

able bonds between precise optical components. The bonds thus formed exhibit the precision and transparency of bonds formed by the conventional optical-contact method and the strength and reliability of high-temperature frit bonds. The method also lends itself to numerous non-optical applications in which there are requirements for precise bonds and/or requirements for bonds, whether precise or imprecise, that can reliably withstand severe environmental condi-

tions. Categories of such non-optical applications include forming composite materials, coating substrates, forming laminate structures, and preparing objects of defined geometry and composition.

The method is applicable to materials that either (1) can form silicatelike networks in the sense that they have silicatelike molecular structures that are extensible into silicatelike networks or (2) can be chemically linked to silicatelike networks by means of hydroxide-



In a **Simple Example of Bonding** according to the present method, a silicon-oxygen-silicon bridge is formed by hydroxide-catalyzed dehydration between two fused-silica substrates, the mating surfaces of which have been hydrated. When a large number of such bridges form, the substrates are bonded together with great strength.

catalyzed hydration and dehydration. When hydrated, a material of either type features surface hydroxyl (—OH) groups. Examples of materials capable of forming silicatelike networks by means of hydroxide-catalyzed hydration and dehydration include several forms of silica (fused silica, fused quartz, and natural quartz), silica-based glasses, silicon having a thermally-grown surface oxide layer, and some other silica-based or silica-containing materials, including some laser crystals. Examples of materials that cannot form silicatelike networks but can be linked to them by means of hydroxide-catalyzed hydration and dehydration include some metals, oxides of some metals, and some non-silica-based, non-silica-containing laser crystals.

In this method, a silicatelike network that bonds two substrates (see figure) can be formed either by a bonding material alone or by the bonding material together with material from either or both of the substrates. In preparation for bonding, the mating surfaces of the substrates should be cleaned to render them maximally hydrophilic or at least minimally hydrophobic. Typically, an

aqueous hydroxide bonding solution is dispensed and allowed to flow between the mating surfaces by capillary action. If at least one of the substrates can form a silicatelike network and if the surface figures of the substrates match with sufficient precision, then a suitable bonding solution would be one that contains a suitable concentration of hydroxide ions but substantially or completely lacks silicate material. If neither substrate material can form a silicatelike network through hydroxide catalysis or if the degree of mismatch between the surface figures of the substrates is such that silicatelike network cannot be formed at a sufficient rate, then a silicate material should be included in the bonding solution.

The solution acts to form a bond within a settling time, during the early part of which one can separate and/or move the substrates to align them more precisely. Regardless of whether substrates to be bonded are capable of forming silicatelike networks or have precisely matching surface figures, the settling time can be tailored via the concentrations of hydroxide ions and silicate material in the bonding solution.

For example, for bonding silica-based materials, the settling time can be tailored between about 40 minutes at one extreme of composition (hydroxide but no silica) and tens of seconds at the other extreme of composition (silica with a smaller proportion of hydroxide).

If the surface figures of the substrates do not match precisely, bonding could be improved by including a filling material in the bonding solution. The filling material could be in the form of particles, foam, and/or a liquid. The filling material facilitates bridging of gaps between the substrate surfaces. Preferably, the filling material should include at least one ingredient that can be hydrated to have exposed hydroxyl groups and that can be chemically linked, by hydroxide catalysis, to a silicatelike network. The silicatelike network could be generated *in situ* from the filling material and/or substrate material, or could be originally present in the bonding material.

This work was done by Dz-Hung Gwo of Stanford University for Marshall Space Flight Center. For more information, contact Sammy Nabors, MSFC Commercialization Assistance Lead, at sammy.a.nabors@nasa.gov. Refer to MFS-32082.



⚙️ **Balanced Flow Meters Without Moving Parts**

These meters perturb flows less than their predecessors do.

Marshall Space Flight Center, Alabama

Balanced flow meters are recent additions to an established class of simple, rugged flow meters that contain no moving parts in contact with flow and are based on measurement of pressure drops across objects placed in flow paths. These flow meters are highly accurate, minimally intrusive, easily manufacturable, and reliable. A balanced flow meter can be easily mounted in a flow path by bolting it between conventional pipe flanges. A balanced flow meter can be used to measure the flow of any of a variety of liquids or gases, provided that it has been properly calibrated.

The innovative aspects and advantages of a balanced flow meter are probably most easily understood by comparing it with its most closely related predecessor, a standard orifice-plate flow meter (see figure). Any flow meter based on the aforementioned pressure-drop principle necessarily introduces some turbulence, permanent pressure loss, and concomitant dissipation of kinetic energy of flow. The turbulence, in turn, introduces a de-

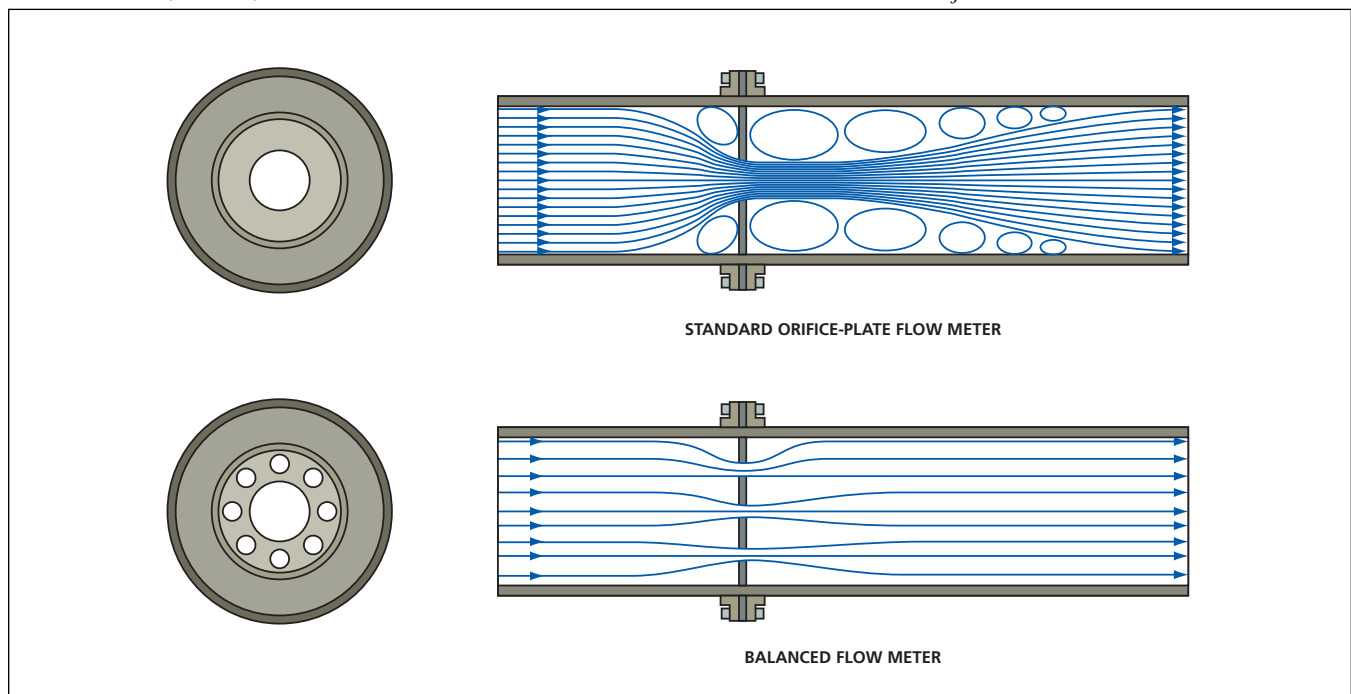
gree of non-repeatability into the measurements and increases the degree of uncertainty of the relation between differential pressure and the flow rate. Relative to the standard orifice-plate flow meter, the balanced flow meter introduces less turbulence and two times less permanent pressure loss and is therefore capable of offering 10 times greater accuracy and repeatability with less dissipation of energy. A secondary benefit of the reduction of turbulence is the reduction of vibration and up to 15 times less acoustic noise generation.

Both the balanced flow meter and the standard orifice-plate flow meter are basically disks that contain holes and are instrumented with pressure transducers on their upstream and downstream faces. The most obvious difference between them is that the standard orifice plate contains a single, central hole while the balanced flow meter contains multiple holes. The term “balanced” signifies that in designing the meter, the sizes and locations of the holes are deter-

mined in an optimization procedure that involves balancing of numerous factors, including volumetric flow, mass flow, dynamic pressure, kinetic energy, all in an effort to minimize such undesired effects as turbulence, pressure loss, dissipation of kinetic energy, and non-repeatability and nonlinearity of response over the anticipated range of flow conditions. Due to proper balancing of these factors, recent testing demonstrated that the balanced flow-meter performance was similar to a Venturi tube in both accuracy and pressure recovery, but featured reduced cost and pipe-length requirements.

This work was done by Anthony R. Kelley of Marshall Space Flight Center and Paul Van-Buskirk of Quality Monitoring and Control.

This invention has been patented by NASA (U.S. Patent No. 7,051,765). Inquiries concerning nonexclusive or exclusive license for its commercial development should be addressed to Sammy Nabors, MSFC Commercialization Assistance Lead, at sammy.a.nabors@nasa.gov. Refer to MFS-31952-1.



The **Flow in the Balanced Flow Meter** is straighter and less turbulent. One consequence is the net pressure loss downstream for the balanced flow meter is less than half that of the standard orifice-plate flow meter.

⚙️ Deflection-Compensating Beam for Use Inside a Cylinder

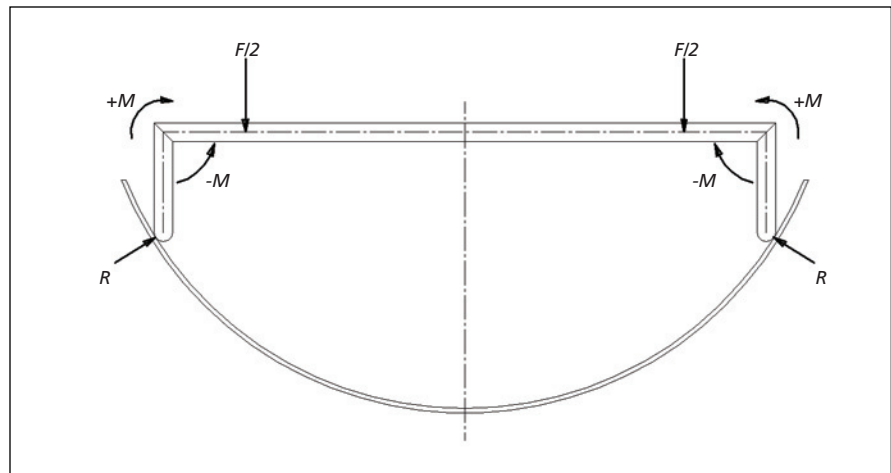
Deflections are minimized by combined effects of the beam and cylinder shapes.

Marshall Space Flight Center, Alabama

A design concept for a beam for a specific application permits variations and options for satisfying competing requirements to minimize certain deflections under load and to minimize the weight of the beam. In the specific application, the beam is required to serve as a motion-controlled structure for supporting a mirror for optical testing in the lower third portion of a horizontal, cylindrical vacuum chamber. The cylindrical shape of the chamber is fortuitous in that it can be (and is) utilized as an essential element of the deflection-minimizing design concept.

The beam is, more precisely, a tablelike structure comprising a nominally flat, horizontal portion with vertical legs at its ends (see figure). The weights of the beam and whatever components it supports are reacted by the contact forces between the lower ends of the legs and the inner cylindrical chamber wall. Whereas the bending moments arising from the weights contribute to a beam deflection that is concave (as viewed from above) with its lowest point at midlength, the bending moments generated by the contact forces acting on the legs contribute to a beam deflection that is convex (as viewed from above) with its highest point at midlength. In addition, the bending of the legs in response to the weights causes the lower ends of the legs to slide downward on the cylindrical wall.

By taking the standard beam-deflection equations, combining them with the geometric relationships among the legs and the horizontal portion of the beam, and treating the sliding as a component of deflection, it is possible to write an equation for the net vertical deflection as a function of the load and of position along the beam:



In this free-body diagram of a **Deflection-Compensating Beam**, F = applied force, M = resulting moment, and R = reaction force.

Total Deflection = (Deflection From Simple Support, Moment Load) + (Deflection From Simple Support, Twin Loads) + (Sliding at Wall)

The following is a summary of major conclusions drawn from the verbal characterization:

- The deflection at the point of application of a load cannot be made zero but it can be reduced, relative to the case of a simply supported beam of equal length.
- It is possible to obtain zero deflection at either the ends of the beam, the midlength point, or two points equidistant from the midlength point.
- The locations of the zero-deflection points are independent of the magnitude of the applied load. Moreover, if the beam and the legs are made of the same material and their cross sections are of the same size and shape, then the locations of the zero-deflection points are independent of the material and the cross sections.

- The maximum stresses occur at the ends of the horizontal portion of the beam.

Yet another advantage of the design concept arises from a fundamental geometric property. Just as a table having three legs of possibly unequal length can always rest on a horizontal surface without wobbling, a table having four legs of possibly unequal length can always rest on a cylindrical surface without wobbling. Hence, one can always be assured of realizing the desired geometry of contact between the beam and the cylindrical wall, and tolerances on leg lengths can be large. Hence, further, the cost of fabrication can be less than it would be if it were necessary to adhere to tight tolerances to ensure the desired geometry of contact.

This work was done by Dwight Goodman, Neill Myers, and Kenneth Herren of Marshall Space Flight Center. For further information, contact Sammy Nabors, MSFC Commercialization Assistance Lead, at sammy.a.nabors@nasa.gov. MFS-32123-1

⚙️ Four-Point-Latching Microactuator

Fabrication is simplified and susceptibility to jamming greatly reduced.

NASA's Jet Propulsion Laboratory, Pasadena, California

Figure 1 depicts an experimental inchworm-type linear microactuator. This microactuator is a successor to the one described in "MEMS-Based Piezoelectric/Electrostatic Inchworm Actuator" (NPO-

30672), *NASA Tech Briefs*, Vol. 27, No. 6 (June 2003), page 68. Both actuators are based on the principle of using a piezoelectric transducer (PZT) operated in alternation with electrostatically actuated

clutches to cause a slider to move in small increments. However, the design of the present actuator incorporates several improvements over that of the previous one. The most readily apparent improvement

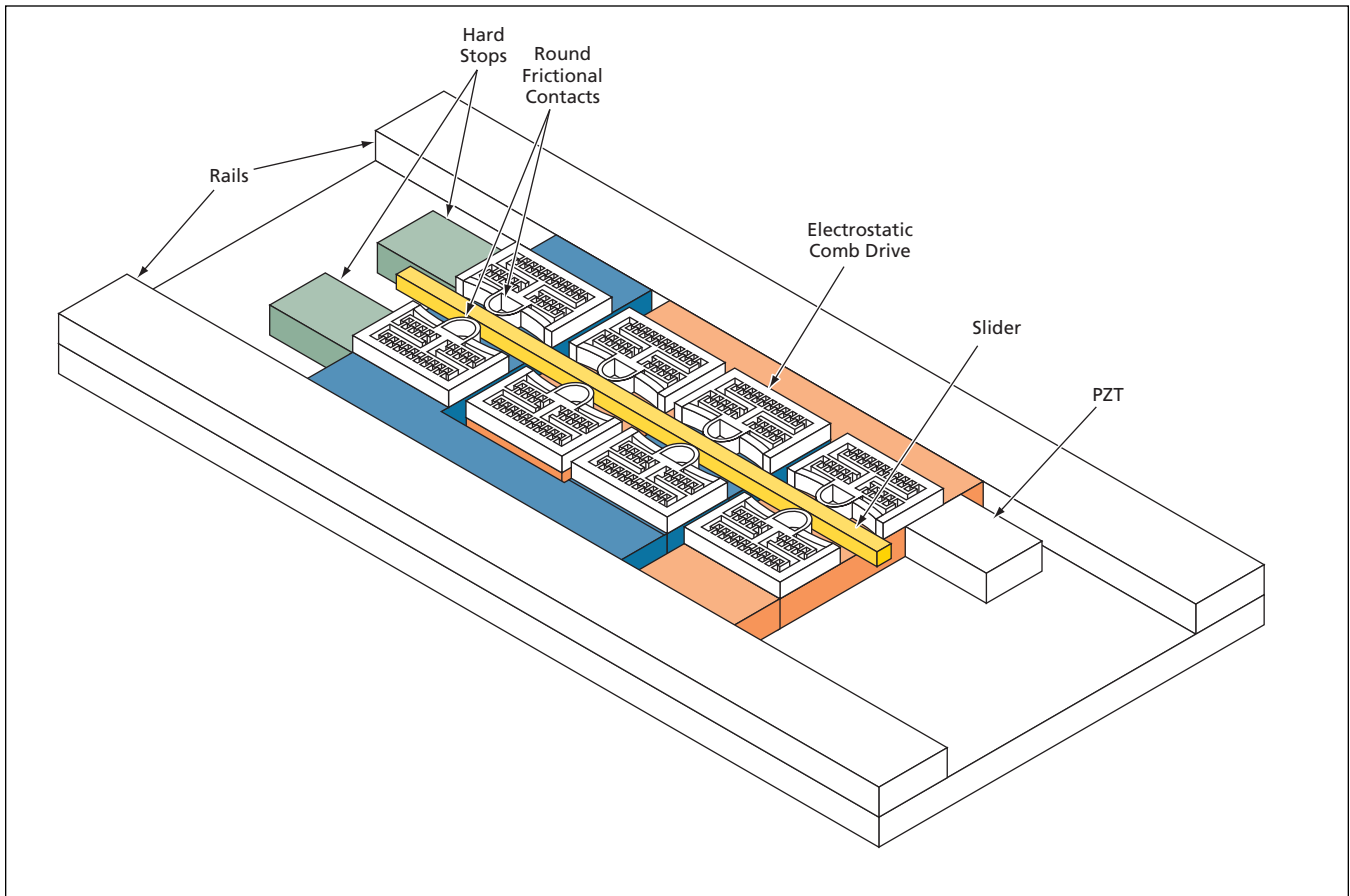


Figure 1. This **Four-Point-Latching Microactuator** features a predominantly planar geometric character and in-plane motion, in contradistinction to a prior microactuator having a more-complex three-dimensional character and perpendicular-to-the-plane motion.

is in geometry and, consequently, in fabrication: In the previous actuator, the inchworm motion was perpendicular to the broad faces of a flat silicon wafer on which the actuator was fabricated, and fabrication involved complex processes to form complex three-dimensional shapes in and on the wafer. In the present actuator, the inchworm motion is parallel to the broad faces of a wafer on which it is fabricated. The components needed to produce the in-plane motion are more nearly planar in character and, consequently, easier to fabricate. Other advantages of the present design are described below.

Whereas the previous actuator contained two clutches (denoted “holders” in the cited prior article), the present actuator contains four clutches. Each clutch includes a pair of units on opposite sides of a channel, into which the slider is inserted and along which the slider moves. Rails along the sides of the substrate prevent outward movement of the clutch units. Each clutch unit includes a rounded frictional contact that is spring-loaded against one side of the slider. Attached to each spring-loaded frictional contact is an electrostatic

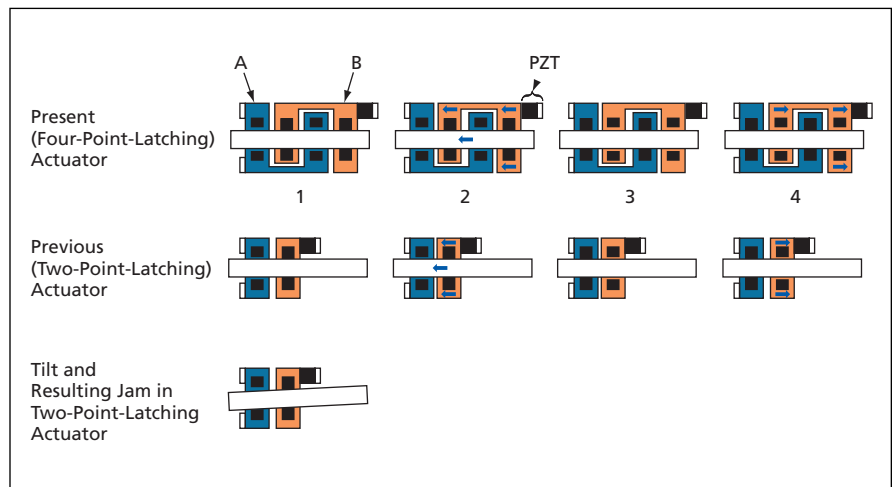


Figure 2. A **PZT and Clutches** are operated in alternation to produce small increments of motion of the slider along its long dimension. In the previous two-clutch actuator, the slider could tilt and become jammed.

comb drive that, when energized, opposes the spring load to pull the contact away from the slider. Hence, each clutch is normally latching: the rounded frictional contacts clamp the slider from opposite sides until and unless the electrostatic comb drives are energized. The spring load is obtained by inserting the slider that is slightly wider than fabri-

cated clutch clearance. This insertion also displaces the comb teeth to achieve very narrow ($<1 \mu\text{m}$) comb gap that is power efficient but difficult to fabricate in bulk Si structure. A low-thermal-expansion-glass lid, omitted from the figure for the sake of clarity, is placed across the rails to retain the slider in the channel.

Figure 2 depicts the operation of the present and previous linear actuators and illustrates one of the advantages of the present actuator over the previous one. In the present actuator, the first and third clutches are operated in unison and are mounted on a stationary structure denoted A. The second and fourth clutches are operated in unison and are mounted on a moveable structure, denoted B, that can be driven a short distance forward or backward along the channel by a PZT. In step 1 of an operational sequence in which the slider is moved leftward, the clutches on unit A are released. In step 2, the PZT is extended to push unit B and the slider leftward. In step 3, the clutches on unit

A are latched while the clutches on unit B are released. In step 4, the PZT is retracted to bring unit B rightward. Repetition of steps 1 through 4 causes the slider to move leftward in repeated small increments.

The operational sequence of the previous two-clutch actuator is similar. However, the two-clutch configuration is susceptible to tilt of the slider and a consequent large increase in drag. Hence, the primary operational advantages of the present four-point-latching design over the prior two-point-latching design are less drag and greater control robustness arising from greater stability of the orientation of the slider.

This work was done by Risaku Toda and Eui-Hyeok Yang of Caltech for NASA's Jet Propulsion Laboratory.

In accordance with Public Law 96-517, the contractor has elected to retain title to this invention. Inquiries concerning rights for its commercial use should be addressed to:

Innovative Technology Assets Management

JPL

Mail Stop 202-233

4800 Oak Grove Drive

Pasadena, CA 91109-8099

(818) 354-2240

E-mail: iaoffice@jpl.nasa.gov

Refer to NPO-42381, volume and number of this NASA Tech Briefs issue, and the page number.

🔧 Curved Piezoelectric Actuators for Stretching Optical Fibers

Curved actuators produce greater displacements than do flat actuators.

Langley Research Center, Hampton, Virginia

Assemblies containing curved piezoceramic fiber composite actuators have been invented as means of stretching optical fibers by amounts that depend on applied drive voltages. Piezoceramic fiber composite actuators are conventionally manufactured as sheets or ribbons that are flat and flexible, but can be made curved to obtain load-carrying ability and displacement greater than those obtainable from the flat versions. A curved actuator of this type can be fabricated by bonding a conventional flexible flat actuator to a thin metal backing sheet in a flat configuration at an elevated temperature so that upon cooling to room temperature, differential thermal contraction of the layers causes the laminate to become curved. Alternatively, such a curved actua-

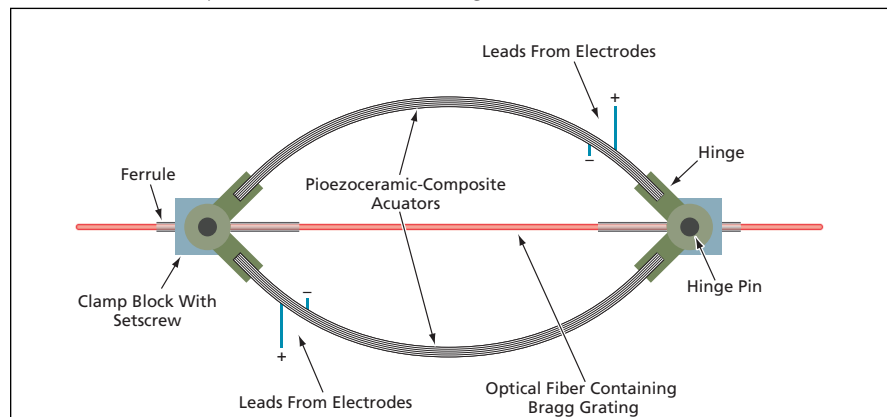
tor can be fabricated by bonding the layers together at room temperature using a curved mold.

In the primary embodiment of this invention, piezoceramic fibers are oriented parallel to the direction of longitudinal displacement of the actuators so that application of drive voltage causes the actuator to flatten, producing maximum motion. Actuator motion can be transmitted to the optical fiber by use of hinges and clamp blocks (see figure). Each clamp block includes a setscrew that tightens down onto a metal ferrule through which the optical fiber is bonded. Each hinge contains a clearance hole for a hinge pin, slots to accept the piezoceramic fiber composite actuators, and a clearance groove for the ferrule.

In the original application of this invention, the optical fiber contains a Bragg grating and the purpose of the controlled stretching of the fiber is to tune the grating as part of a small, lightweight, mode-hop-free, rapidly tunable laser for demodulating strain in Bragg-grating strain-measurement optical fibers attached to structures. The invention could also be used to apply controllable tensile force or displacement to an object other than an optical fiber.

Prior tunable lasers that are not fiber-optic lasers are relatively bulky and are limited to tuning frequencies of the order of 1 Hz. Tunable fiber-optic lasers could potentially be made much smaller, lighter in weight, and more rapidly tunable if strained by use of this invention. Prior actuators that could be used to strain-tune fiber-optic lasers or gratings include piezoelectric stacks that produce displacements smaller than those needed and that, in comparison with assemblies according to the present invention, are heavier. Displacements produced by piezoelectric stacks can be amplified mechanically, but the mechanisms needed to effect amplification add considerable weight, which can be unacceptable in aeronautical or aerospace applications because of the high per-unit-weight cost of flight.

This work was done by Sidney G. Allison, Qamar A. Shams and Robert L. Fox of Langley Research Center. For further information, contact the Langley Innovative Partnerships Office at (757) 864-4015. LAR-17356-1



An Assembly Containing Two Curved Actuators stretches an optical fiber by an amount that depends on the voltage applied to the electrodes.

🔧 Tunable Optical Assembly With Vibration Dampening

Flat actuators are mechanically simple and offer vibration dampening.

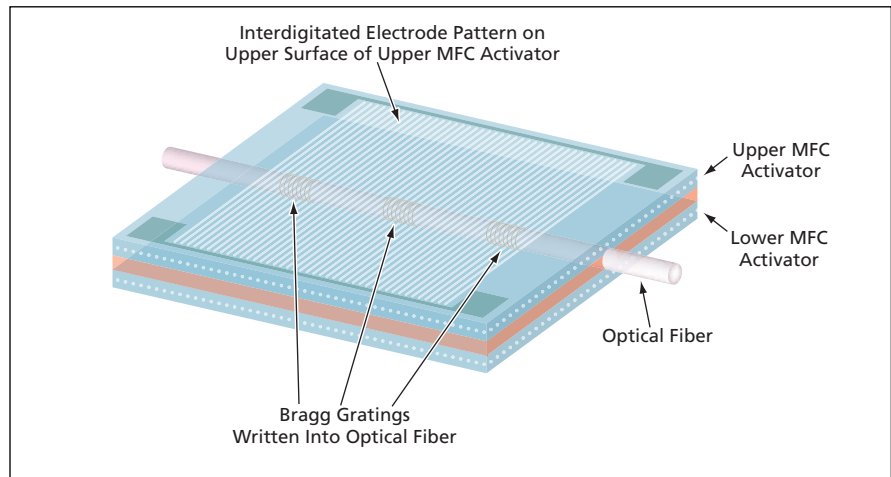
Langley Research Center, Hampton, Virginia

Since their market introduction in 1995, fiber Bragg gratings (FBGs) [wherein “fiber” signifies optical fiber] have emerged as excellent means of measuring such parameters as strain and temperature. Distributed-grating sensing is particularly beneficial for such structural-health monitoring applications such as those of “smart” structures or integrated vehicle health management in aerospace vehicles. Because of the variability of their output wavelengths, tunable lasers have become widely used as means of measuring FBGs.

Several versions of a lightweight assembly for strain-tuning an FBG and dampening its vibrations have been constructed. The main components of such an assembly are one or more piezoelectric actuators, an optical fiber containing one or more Bragg grating(s), a Bragg-grating strain-measurement system, and a voltage source for actuation. The piezoelectric actuators are, more specifically, piezoceramic fiber composite actuators and, can be, still more specifically, of a type known in the art as macro-fiber composite (MFC) actuators. In fabrication of one version of the assembly, the optical fiber containing the Bragg grating(s) is sandwiched between the piezoelectric actuators (see figure) along with an epoxy that is used to bond the optical fiber to both actuators, then the assembly is placed in a vacuum bag and kept there until the epoxy is cured.

Two other versions of the assembly can be characterized as follows:

- During the fabrication of one of the piezoelectric actuators, the optical fiber containing the Bragg grating(s) is embedded in the actuator in place of one of



In This Tunable Optical Assembly, an optical fiber containing Bragg gratings is sandwiched between two MFC actuators.

the piezoceramic fibers.

- The surface of an MFC actuator is roughened by sandblasting to improve subsequent bonding, then the optical fiber containing the Bragg grating(s) is bonded to the roughened surface by use of an adhesive.

In operation of any version of the assembly, when the optical fiber is strained by the actuator(s), the wavelength of light reflected from the Bragg grating(s) changes by an amount that depends on the amount of strain. This method of straining an optical fiber containing Bragg gratings to produce a shift in the reflected wavelength holds promise because it may also be useful for tuning an optical-fiber laser.

Bonding an FBG directly into an MFC actuator greatly reduces the complexity, relative to assemblies, of the type described

in the immediately preceding article, that include piezoceramic fiber composite actuators, hinges, ferrules, and clamp blocks with setscrews. Unlike the curved actuators, MFC actuators are used in a flat configuration and are less bulky than are the assemblies described in the immediately preceding article. In addition, the MFC offers some vibration dampening and support for the optical fiber whereas, in an assembly of the type described in the immediately preceding article, the optical fiber is exposed, and there is nothing to keep the exposed portion from vibrating.

This work was done by Qamar A. Shams, Sidney G. Allison, and Robert L. Fox of Langley Research Center. Further information is contained in a TSP (see page 1).

LAR-17073-1

🔧 Passive Porous Treatment for Reducing Flap Side-Edge Noise

Advantages include broadband noise reduction with no aerodynamic-lift penalty.

Langley Research Center, Hampton, Virginia

A passive porous treatment has been proposed as a means of suppressing noise generated by the airflow around the side edges of partial-span flaps on airplane wings when the flaps are extended in a high-lift configuration. The treatment proposed here does not incur any aerodynamic penalties and could easily be retrofit to existing airplanes.

The treatment could also be applied to reduce noise generated by turbomachinery, including wind turbines. Innovative aspects of the proposed treatment include a minimum treatment area and physics-based procedure for treatment design. The efficacy of the treatment was confirmed during wind-tunnel experiments at NASA Ames, wherein the

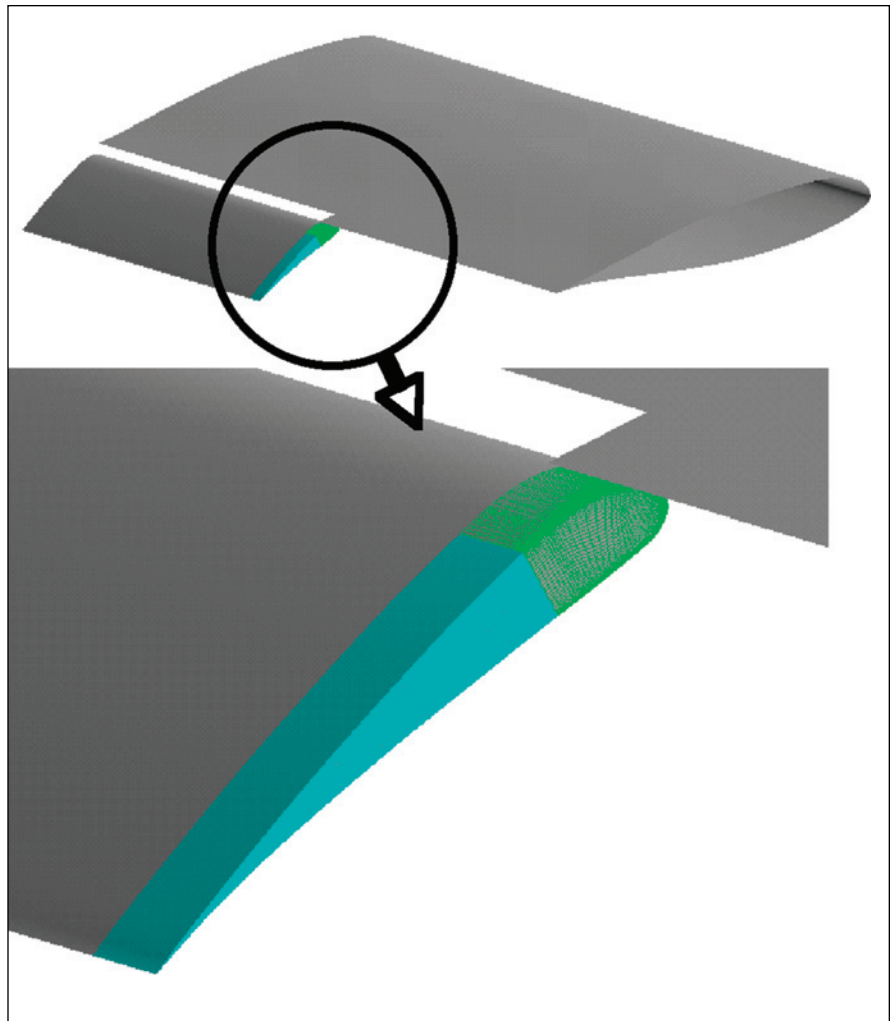
porous treatment was applied to a minute surface area in the vicinity of a flap edge on a 26-percent model of Boeing 777-200 wing.

The flap side-edge noise constitutes a significant portion of the overall airframe noise during descent and landing of an aircraft. The acoustically relevant flow features at typical flap side edges

consist of free shear layers, the roll-up of these layers to form multiple vortices, merging of vortices, and, at high flap deflections, breakdown of these vortices. Because of their unsteadiness and their proximity to flap side-edge surface, these features can contribute to the noise radiated from the flap side edges. To be effective, any treatment for reducing the flap side-edge noise must eliminate, reduce, or alter the vortex initiation regime and the intensity of the vortex roll up and/or breakdown process near the side edge of the flap.

According to the proposal, small, carefully selected areas in the flap-tip regions of each flap would be rendered porous by use of materials similar to those used for wall cooling of turbine blades or the materials used towards acoustical treatment of aircraft-engine ducts (see figure). Porosity at the tips would provide a means of communication between the flow over the lower, side, and upper surfaces near the edge of the flap and, hence, modify the vortex structures near the tip.

Unlike side-edge fences that have been investigated for reduction of flap side-edge noise, the proposed treatment would not incur extra weight and is not likely to accrue drag penalty during the cruise phase of the flight. Unlike the porous tip treatments considered previously in a cut-and-try approach, the proposed porous tip treatment is based on comprehensive analysis of the acoustically relevant features of the flow field and, consequently, would be amenable to optimization. The airflow around the side edges of the flaps can be simulated using computational fluid dynamics (CFD), and results of CFD simulations can be combined with simplified math-



Model Geometry and Schematic of Treated Surfaces are shown. The cyan region depicts the aft-only configuration; the green mesh shows the additional area included in the leading-edge configurations.

ematical models of candidate porous treatments to analyze the effectiveness of the treatment in a specific application. Minimization of the amount of area that must be treated in order to reduce the flap side-edge noise to an ac-

ceptable degree could be an integral part of the design optimization process.

This work was done by Meelan M. Choudhari and Mehdi R. Khorrami of Langley Research Center. Further information is contained in a TSP (see page 1). LAR-16302-1

⚙️ Cylindrical Piezoelectric Fiber Composite Actuators

Cylindrical actuators offer advantages over flat flexible actuators.

Langley Research Center, Hampton, Virginia

The use of piezoelectric devices has become widespread since Pierre and Jacques Curie discovered the piezoelectric effect in 1880. Examples of current applications of piezoelectric devices include ultrasonic transducers, micro-positioning devices, buzzers, strain sensors, and clocks. The invention of such lightweight, relatively inexpensive piezoceramic-fiber-composite actuators as

macro fiber composite (MFC) actuators has made it possible to obtain strains and displacements greater than those that could be generated by prior actuators based on monolithic piezoceramic sheet materials. MFC actuators are flat, flexible actuators designed for bonding to structures to apply or detect strains. Bonding multiple layers of MFC actuators together could increase force capa-

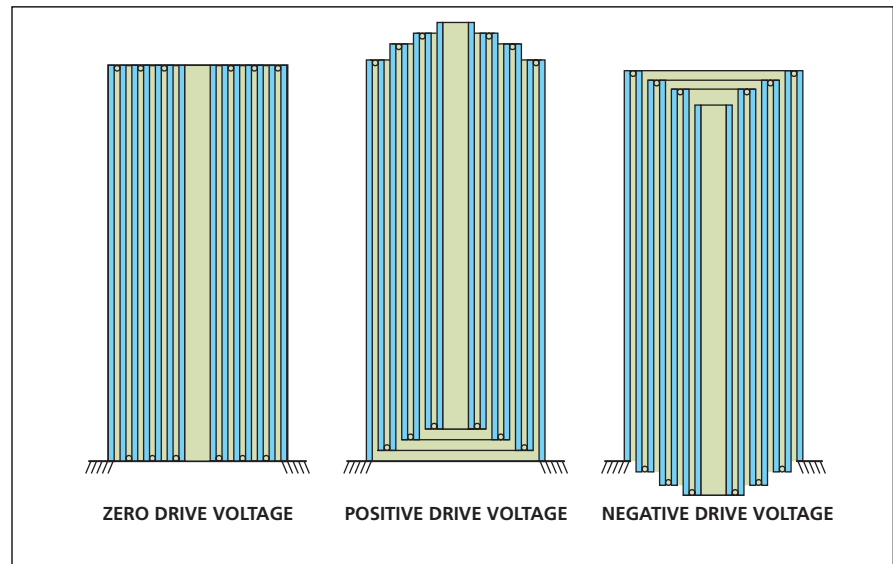
bility, but not strain or displacement capability.

Cylindrical piezoelectric fiber composite (CPFC) actuators have been invented as alternatives to MFC actuators for applications in which greater forces and/or strains or displacements may be required. In essence, a CPFC actuator is an MFC or other piezoceramic fiber composite actuator fabricated in a cylindrical instead of

its conventional flat shape. “Cylindrical” is used here in the general sense, encompassing shapes that can have circular, elliptical, rectangular or other cross-sectional shapes in the planes perpendicular to their longitudinal axes. CPFC actuators retain the desirable high strain or displacement and multiple-layer force enhancement capabilities of conventional flat piezoceramic fiber composite actuators. An advantage of the cylindrical over the flexible flat actuators is that the cylindrical shapes impart stiffness, so that unlike the flat actuators, the cylindrical actuators can bear loads even when they are not attached to supporting structures.

Another advantage of the cylindrical over the flexible flat actuators is that displacements of multiple CPFC actuators can be added together. For this purpose, CPFC actuators having different diameters can be assembled in a concentric telescoping arrangement and joined at alternating ends, as shown in the figure. Application of positive drive voltage causes the assembly to elongate in one direction; application of a negative drive voltage causes the assembly to elongate in the opposite direction.

CPFC actuators were first conceived as an improved means of strain-tuning optical-fiber Bragg gratings for applications involving tunable lasers. The ability to add the displacements of multiple self-stiffening CPFC actuators affords greatly enhanced strain-tuning range while still mak-



CPFC Actuators in a concentric telescoping arrangement are depicted here in meridional cross sections under three different drive-voltage conditions to illustrate how displacements are added.

ing it possible for strain-tuning assemblies to be compact and lightweight. However, CPFC actuators have potential utility in a broad range of applications beyond those involving tunable lasers. For example, CPFC actuator assemblies might supplant piezoelectric stacks in some applications, particularly those in which lighter weight and enhanced displacement are desirable.

In comparison with CPFC actuators, piezoelectric stacks are heavier and produce much smaller displacements. Displacements produced by piezoelectric

stacks can be amplified mechanically, but the mechanisms needed to effect amplification have considerable weight. Other actuators capable of larger displacements include hydraulic or gas piston-cylinder actuators, which are heavier and must be accompanied by supplies of pressurized hydraulic fluids or gases.

This work was done by Sidney G. Allison, Qamar A. Shams and Robert L. Fox of Langley Research Center. For further information, contact the Langley Innovative Partnerships Office at (757) 864-4015. LAR-17168-1



Patterning of Indium Tin Oxide Films

The patterns are formed by laser printing directly onto the films.

John F. Kennedy Space Center, Florida

A relatively rapid, economical process has been devised for patterning a thin film of indium tin oxide (ITO) that has been deposited on a polyester film. ITO is a transparent, electrically conductive substance made from a mixture of indium oxide and tin oxide that is commonly used in touch panels, liquid-crystal and plasma display devices, gas sensors, and solar photovoltaic panels. In a typical application, the ITO film must be patterned to form electrodes, current collectors, and the like. Heretofore it has been common practice to pattern an ITO film by means of either a laser ablation process or a photolithography/etching process. The laser ablation process includes the use of expensive equipment to precisely position and focus a laser. The photolithography/etching process is time-consuming.

The present process is a variant of the direct toner process — an inexpensive but often highly effective process for patterning conductors for printed circuits. Relative to a conventional photolithography/etching process, this process is simpler, takes less time, and is less ex-

pensive. This process involves equipment that costs less than \$500 (at 2005 prices) and enables patterning of an ITO film in a process time of less than about a half hour.



A Pattern of Interdigitated Electrodes was formed directly on the ITO-coated surface of a transparent polyester film by use of a laser printer. After etching away of the ITO not covered by the toner, the toner was washed away, leaving the polyester film with the patterned ITO.

In the direct toner process as practiced heretofore, a laser printer or copier is used to print the desired pattern on a water-soluble paper, from whence the pattern is transferred to a circuit board in a sequence of laminating, lift-off, and etching steps. In the present variant of the direct toner process, there is no need for transfer paper: instead, an ITO-coated polyester film is fed directly into a laser printer or copier, where the pattern is printed directly onto the ITO. The patterned polyester film (see figure) is then immersed in a 10-percent (2-normal) solution of H_2SO_4 in water. The sulfuric acid etches away the ITO in the non-printed areas, while the toner in the printed pattern serves as a mask to prevent etching of the underlying ITO. After etching, the toner is washed away by use of acetone, leaving the patterned ITO.

*This work was done by Christopher Immer of ASRC Aerospace Corp. for Kennedy Space Center. Further information is contained in a TSP (see page 1).
KSC-12828*

Gimbaled Shoulders for Friction Stir Welding

Digging of edges of shoulders into workpieces would be reduced or eliminated.

Marshall Space Flight Center, Alabama

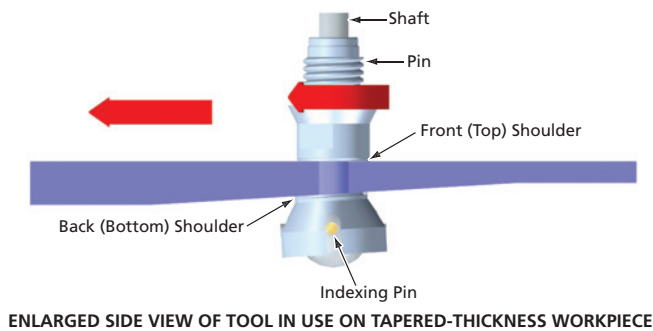
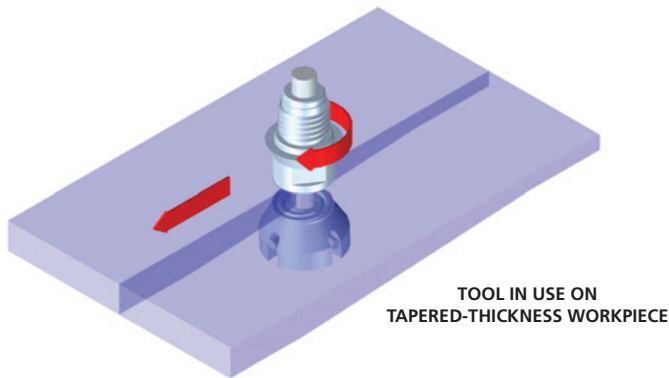
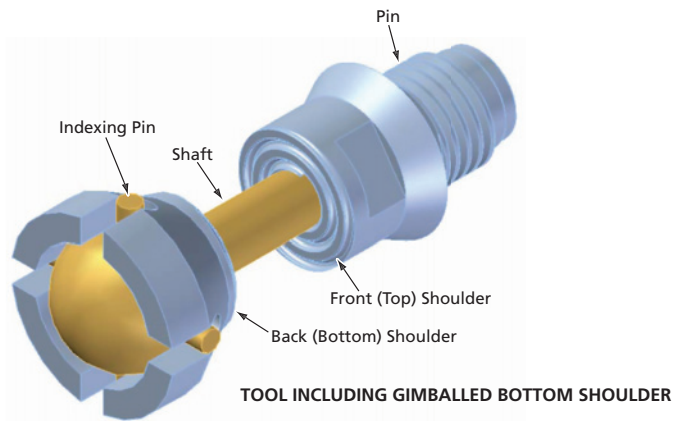
In a proposed improvement of tooling for friction stir welding, gimbaled shoulders would supplant shoulders that, heretofore, have been fixedly aligned with pins. The proposal is especially relevant to self-reacting friction stir welding.

Some definitions of terms, recapitulated from related prior *NASA Tech Briefs* articles, are prerequisite to a meaningful description of the proposed improvement. In friction stir welding, one uses a tool that includes (1) a rotating shoulder on top (or front) of the workpiece and (2) a pin that rotates with the shoulder and protrudes from the shoulder into the

depth of the workpiece. In conventional friction stir welding, the main axial force exerted by the tool on the workpiece is reacted through a ridged backing anvil under (behind) the workpiece. When conventional friction stir welding is augmented with an auto-adjustable pin-tool (APT) capability, the depth of penetration of the pin into the workpiece is varied in real time by a position- or force-control system that extends or retracts the pin as needed to obtain the desired effect.

In self-reacting (also known as self-reacted) friction stir welding as practiced heretofore, there are two shoulders: one

on top (or front) and one on the bottom (or back) of the workpiece. In this case, a threaded shaft protrudes from the tip of the pin to beyond the back surface of the workpiece. The back shoulder is held axially in place against tension by a nut on the threaded shaft. Both shoulders rotate with the pin and remain aligned coaxially with the pin. The main axial force exerted on the workpiece by the tool and front shoulder is reacted through the back shoulder and the threaded shaft into the friction-stir-welding machine head, so that a backing anvil is no longer needed. A key transmits torque between the bottom shoulder and the threaded



The Back Shoulder Would be Gimballed to accommodate local variations in the slope of the lower surface of the workpiece.

shaft, so that the bottom shoulder rotates with the shaft. This concludes the prerequisite definitions of terms.

One consequence of the fixed alignment of the shoulders with the pin is that if the thickness of the workpiece or the slope of either surface of the workpiece varies as the tool moves along the workpiece, then the leading or trailing edge(s) of one or both shoulder(s) tend to dig into the workpiece, generating excessive flashing along the weld. The proposed improvement would be a simple, relatively inexpensive means of preventing or reducing such digging. The gimbaling of either or both shoulder(s) would enable the tool to better adapt to curvatures and other local variations in the slopes of workpiece surfaces, without need for a complex, expensive shoulder-angle control system.

The figure depicts a representative tool for self-reacting friction stir welding incorporating the proposed improvement. [In this case, the bottom shoulder (only) would be gimballed. Optionally, both shoulders or the top shoulder (only) could be gimballed.] The shaft would be terminated in a ball, from which indexing pins would protrude radially at angular intervals of 90° in a plane perpendicular to the pin/shaft axis. The indexing pins would define gimbal axes. The bottom shoulder would contain slots that would loosely engage the indexing pins. The configuration of the indexing pins and slots would be such that the bottom shoulder would be forced to rotate with the pin and shaft and the pins would hold the back (bottom) shoulder axially in place against tension, yet the looseness of the pin/slot engagement would allow limited rotation of the bottom shoulder about the gimbal axes to accommodate local variations in the slope of the lower surface of the workpiece.

This work was done by Robert Carter and Kirby Lawless of Marshall Space Flight Center.

This invention is owned by NASA, and a patent application has been filed. For further information, contact Sammy Nabors, MSFC Commercialization Assistance Lead, at sammy.a.nabors@nasa.gov. Refer to MFS-32115-1.



Improved Thermal Modulator for Gas Chromatography

Varying temperature can be controlled precisely at relatively low power demand.

Goddard Space Flight Center, Greenbelt, Maryland

An improved thermal modulator has been invented for use in a variant of gas chromatography (GC). The variant in question — denoted as two-dimensional gas chromatography (2DGC) or GC-GC — involves the use of three series-connected chromatographic columns, in the form of capillary tubes coated interiorly with suitable stationary phases (compounds for which different analytes exhibit different degrees of affinity). The two end columns are relatively long and are used as standard GC columns. The thermal modulator includes the middle column, which is relatively short and is not used as a standard GC column: instead, its temperature is modulated to affect timed adsorption and desorption of analyte gases between the two end columns in accordance with a 2DGC protocol.

In general, what is required of a thermal modulator is to vary the tempera-

ture of the middle capillary tube in the following cycle:

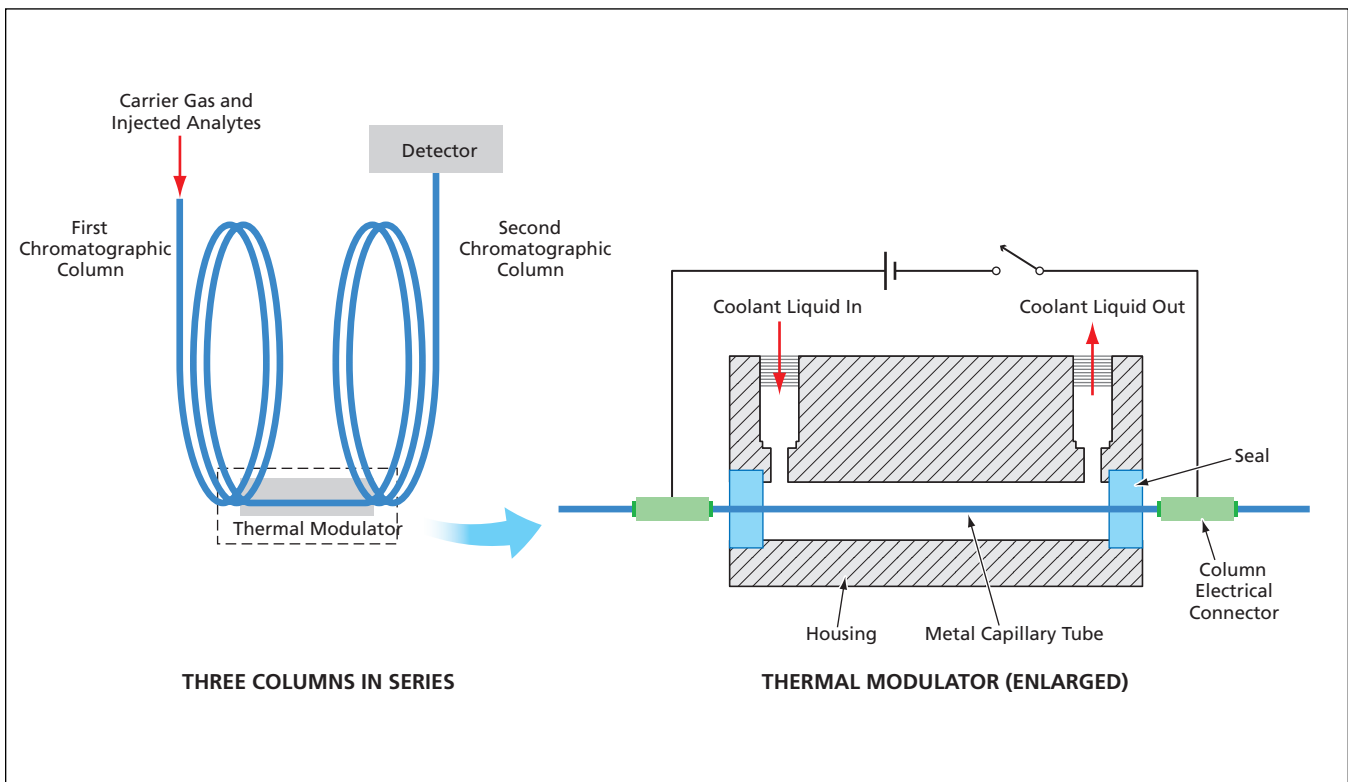
1. Maintain the tube at a specified low temperature — typically between -10 and -40 °C for a specified time (typically between 1 and 10 seconds);
2. Heat (within tens of milliseconds) the tube to a specified high temperature (typically between 180 and 350 °C) and maintain this temperature for a specified time (typically between 10 and 200 milliseconds); then
3. Cool (preferably within 200 milliseconds) the tube back to the low temperature.

The degree to which this heating-and-cooling profile can be exactly controlled can have significant effects on performance, because of an exponential dependence of gas-elution speed on modulator temperature.

What distinguishes the present thermal modulator from prior thermal modulators

is an improved design that enables the required rapid cyclic heating and cooling with greater precision of temperature control and less power demand. The capillary tube is made of metal coated on its inner surface with a protective layer and a suitable stationary phase. Along most of its length, the tube lies in a cylindrical cavity in a housing (see figure). Rapid cooling is achieved through contact between the tube and a coolant liquid that is continuously pumped through the cavity. Rapid heating is achieved by passing a controlled electric current along the tube.

Because of the large radial temperature gradient occasioned by the narrowness of the capillary tube (typically no more than 2 mm wide) and the presence of coolant liquid in contact with the tube, it is difficult or impossible to measure the temperature of the tube accurately by use of a thermocouple, thermistor, or other conventional temperature



In the **Thermal Modulator**, the capillary tube is heated ohmically and is in direct contact with a circulating coolant liquid. The electrical resistance of the tube is used as temperature feedback for controlling the applied voltage or current to obtain the desired temperature-versus-time profile.

sensor. In the improved design, no attempt is made to use a conventional temperature sensor. Instead, for purposes of monitoring and feedback control of the temperature, the electrical resistance of the tube is measured as a function of time and the temperature is computed in real time by use of temperature-vs.-re-

sistance data obtained in prior calibration measurements on the tube.

This work was done by Ernest Frederick Haselbrink, Jr.; Patrick J. Hunt, and Richard D. Sacks of the University of Michigan for Goddard Space Flight Center.

In accordance with Public Law 96-517, the contractor has elected to retain title to this

invention. Inquiries concerning rights for its commercial use should be addressed to:

*University of Michigan
2350 Hayward Street Room 2150
Ann Arbor, MI 48019*

Refer to GSC-14855-1, volume and number of this NASA Tech Briefs issue, and the page number.

Nuclear-Spin Gyroscope Based on an Atomic Co-Magnetometer

Sensitivity to magnetic fields is eliminated.

John H. Glenn Research Center, Cleveland, Ohio

An experimental nuclear-spin gyroscope is based on an alkali-metal/noble-gas co-magnetometer, which automatically cancels the effects of magnetic fields. Whereas the performances of prior nuclear-spin gyroscopes are limited by sensitivity to magnetic fields, this gyroscope is insensitive to magnetic fields and to other external perturbations. In addition, relative to prior nuclear-spin gyroscopes, this one exhibits greater sensitivity to rotation. There is commercial interest in development of small, highly sensitive gyroscopes. The present experimental device could be a prototype for development of nuclear-

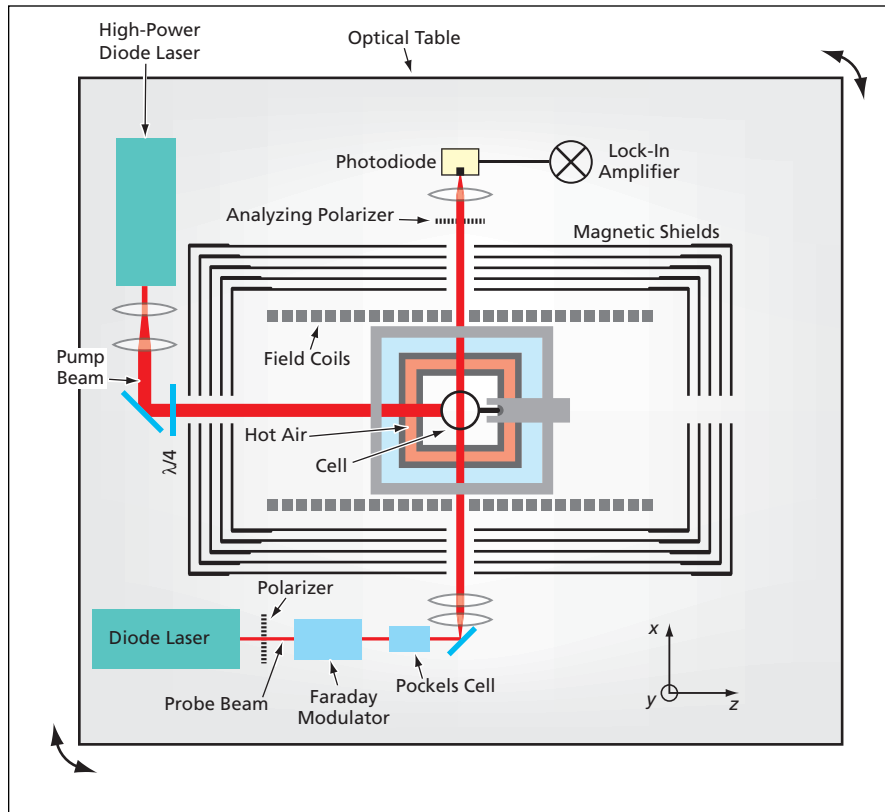
spin gyroscopes suitable for navigation. In comparison with fiber-optic gyroscopes, these gyroscopes would draw less power and would be smaller, lighter, more sensitive, and less costly.

The co-magnetometer (see figure) includes a spherical aluminosilicate glass cell containing potassium vapor, several atmospheres of helium-3, and a small quantity of nitrogen (which serves as a buffer gas). The cell resides in a small oven, which is used to maintain the cell contents at a temperature of 170 °C. The oven is located within a housing that includes several layers of magnetic shielding.

Potassium atoms are polarized by optical pumping, and the polarization is transferred to the helium by spin-exchange collisions. A high-power diode laser generates the pump beam, which passes through holes in the magnetic-shielding layers and oven and through the cell along the z axis of an xyz Cartesian coordinate system. Another, lower-power diode laser generates a linearly polarized probe beam, which similarly passes through the cell along the z axis. The probe beam is used to measure the direction of polarization of the electrons in the potassium atoms, which is coupled to the nuclear polarization of the helium due to the imaginary part of the spin-exchange cross-section.

For sufficiently high buffer-gas pressure in a spherical cell, this coupling can be represented by an effective magnetic field that each spin species (K or He) experiences from the average magnetization of the other.

It has been shown that the relationships among the electron polarization of the potassium atoms, the nuclear polarization of the helium atoms, the magnetic fields, and the mechanical rotation of the magnetometer are described by a system of coupled Bloch equations. The equations have been solved to obtain an equation for (1) a compensating magnetic field, automatically generated in the magnetometer, that exactly cancels other magnetic fields; and (2) a gyroscope output signal that is proportional to the rate of mechanical rotation about the y axis and independent of magnetic fields. In experiments, the gyroscope-output equation has been verified to within a calibration error of 3 percent, and the expected insensitivity to rotation about the x and z axes was confirmed. In a future version, sensitivity could be increased by substitut-



This **Atomic Co-Magnetometer** generates an output signal proportional to the rate of rotation about the y axis.

ing ^{21}Ne for ^3He as the noble gas and increasing the sensitivity of optical measurement of rotation of polarization at low frequencies to approach the spin-projection noise.

This work was done by Michael Romalis, Tom Kornack, and Rajat Ghosh of Princeton University for Glenn Research Center. Further information is contained in a TSP (see page 1). Inquiries concerning rights for the commercial use of this invention should be addressed to NASA Glenn Research Center, Innovative Partnerships Office, Attn: Steve Fedor, Mail Stop 4-8, 21000 Brookpark Road, Cleveland, Ohio 44135. Refer to LEW-17942-1.

This work was done by Michael Romalis, Tom Kornack, and Rajat Ghosh of Princeton University for Glenn Research Center. Further information is contained in a TSP (see page 1). Inquiries concerning rights for the commercial use of this invention should be addressed to NASA Glenn Research Center, Innovative Partnerships Office, Attn: Steve Fedor, Mail Stop 4-8, 21000 Brookpark Road, Cleveland, Ohio 44135. Refer to LEW-17942-1.

Utilizing Ion-Mobility Data To Estimate Molecular Masses

Potential applications include detecting biochemicals in pharmaceutical settings.

NASA's Jet Propulsion Laboratory, Pasadena, California

A method is being developed for utilizing readings of an ion-mobility spectrometer (IMS) to estimate molecular masses of ions that have passed through the spectrometer. The method involves the use of (1) some feature-based descriptors of structures of molecules of interest and (2) reduced ion mobilities calculated from IMS readings as inputs to (3) a neural network. This development is part of a larger effort to enable the use of IMSs as relatively inexpensive, robust, lightweight instruments to identify, via molecular masses, individual compounds or groups of compounds (especially organic compounds) that may be present in specific environments or samples. Potential applications include detection of organic molecules as signs of life on remote planets, modeling and detection of biochemicals of interest in the pharmaceutical and agricultural industries, and detection of chemical and biological hazards in industrial, homeland-security, and industrial settings.

The following background information is prerequisite to a meaningful summary of the present method.

- An IMS includes a drift tube that has length L and is filled with a drift gas (e.g., N_2 or CO_2) at a pressure, P , which could be atmospheric or any other suitable pressure. Mixed into the drift gas is a trace amount of ionized molecules from a sample or environment of interest. An electric potential (V) is applied between the ends of the drift tube.
- The mobility (K) of the ions is given by $K \equiv L^2/Vt$, where t is the amount of time taken by the ions to drift along the tube from the inlet to a detector at the outlet.
- The correlation among the mobility, the mass (m) of an ion, the mass (M) of a drift-gas molecule, and the cross section (Ω) for collisions between an ion and a drift-gas molecule is given

by

$$K = \frac{3q}{16N} \left(\frac{2\pi}{kT} \right)^{1/2} \left(\frac{m+M}{mM} \right)^{1/2} \frac{1}{\Omega}$$

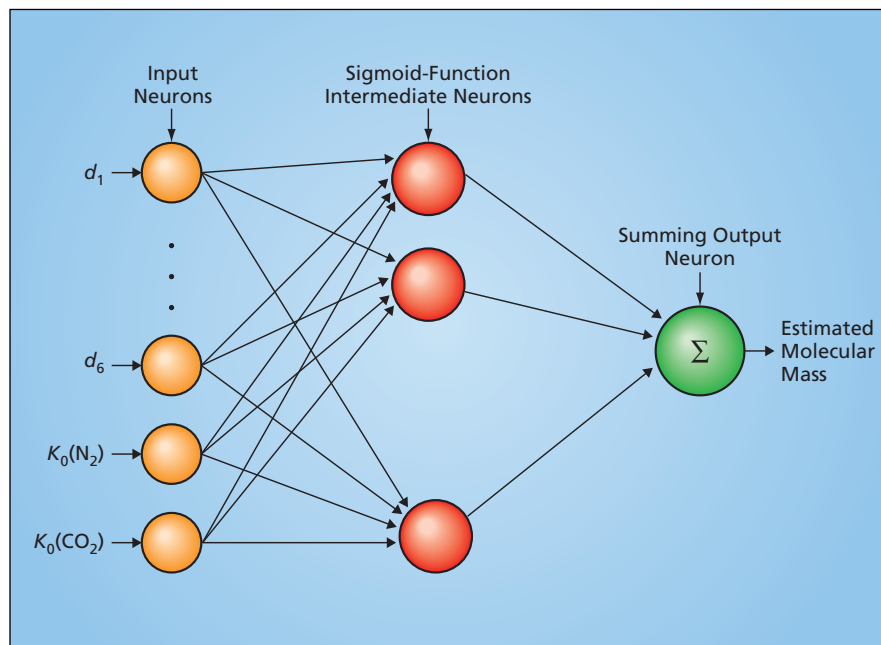
where q is the fundamental unit of electric charge, N is the density of the drift-gas molecules, and k is Boltzmann's constant.

- The reduced mobility (K_0) is given by $K_0 \equiv KT_S P / TP_S$, where T_S denotes standard temperature (≈ 273 K) and P_S is standard atmospheric pressure (represented by a mercury-barometer column height of 760 mm under normal Earth gravitation).
- In a previous study, it was found that there are some correlations between the molecular structure of each compound and the K_0 value of ions of that compound in a given drift gas.

This concludes the background information.

The theoretical basis of the present developmental method can be summa-

rized as the hypotheses that there could be a correlation among molecular structure, collision cross section, and molecular mass, such that it should be possible to estimate the mass of an ion by $m = \Phi(K_0)$, where Φ is a nonlinear function to be determined, $\hat{\Omega}$ is an estimated collision cross section that one strives to make as nearly equal as possible to the observed collision cross section. The estimated collision cross section is expressed as $\hat{\Omega} = g(W, S)$, g is another nonlinear function to be determined, W is a vector of weights in a parameter space (e.g., a vector of neural-network weights), and $S \equiv (d_1, d_2, d_3, \dots)$ is a vector of feature-based numerical descriptors of the molecular structure. In this method, the applicable equations are not solved explicitly; rather, they are solved implicitly by means of a neural network (see figure). For each compound of interest, the inputs to the neural network are (1) a set of six feature-based descriptors extracted from a



A Neural Network processes six feature-based descriptors (d_1 through d_6) and reduced-mobility values for two drift gases [$K_0(\text{N}_2)$ and $K_0(\text{CO}_2)$] into an estimate of molecular mass.

much larger set of molecular-structure descriptors by means of principal-component analysis and (2) K_0 values for that compound in two different drift gases.

In a numerical-simulation test of the method, the neural network was trained

by use of descriptors, K_0 values, and molecular masses pertaining to 65 organic compounds, then interrogated by use of descriptors and K_0 values pertaining to 10 other organic compounds. The molecular masses generated by the neural network were found to differ from the

correct values by root-mean-square errors of no more than a few percent.

This work was done by Tuan Duong and Isik Kanik of Caltech for NASA's Jet Propulsion Laboratory. Further information is contained in a TSP (see page 1). NPO-44576

Optical Displacement Sensor for Sub-Hertz Applications

NASA's Jet Propulsion Laboratory, Pasadena, California.

A document discusses a sensor made from off-the-shelf electro-optical photodiodes and electronics that achieves $20 \text{ nm}/(\text{Hz})^{1/2}$ displacement sensitivity at 1 mHz. This innovation was created using a fiber-coupled laser diode (or Nd:YAG) through a collimator and an aperture as the illumination source. Together with a germanium quad photodiode, the above-mentioned displace-

ment sensor sensitivities have been achieved. This system was designed to aid the Laser Interferometer Space Antenna (LISA) with microthruster tests and to be a backup sensor for monitoring the relative position between a proof mass and a spacecraft for drag-free navigation. The optical displacement sensor can be used to monitor any small displacement from a remote loca-

tion with minimal invasion on the system.

This work was done by Alexander Abramovici, Meng P. Chiao, and Frank G. Dekens of Caltech for NASA's Jet Propulsion Laboratory. For further information, download the Technical Support Package (free white paper) at www.techbriefs.com/tsp under the Physical Sciences category. NPO-30681

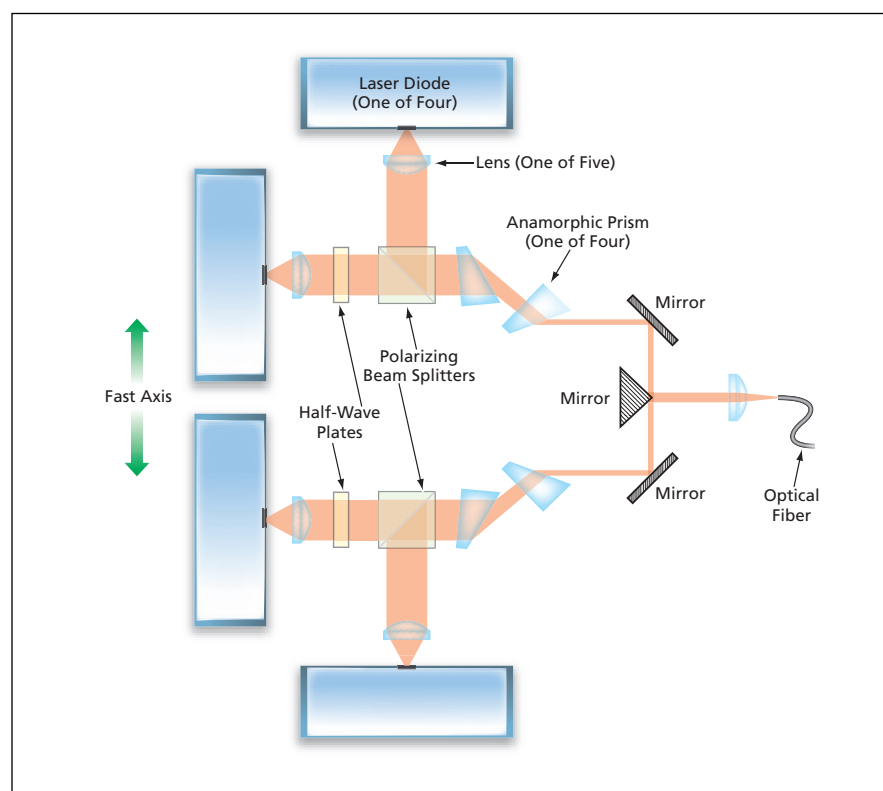
Polarization/Spatial Combining of Laser-Diode Pump Beams

Four beams are combined into two, which are then combined into one.

NASA's Jet Propulsion Laboratory, Pasadena, California

The figure depicts a breadboard version of an optical beam combiner that makes it possible to use the outputs of any or all of four multimode laser diodes to pump a non-planar ring oscillator (NPRO) laser. This apparatus could be an alternative to the one described in the immediately preceding article. Whereas that one utilizes spatial (beam-shaping) beam-combining techniques, this one utilizes a combination of polarization and spatial beam-combining techniques. In both that case and this one, the combined multiple laser-diode pump beams are coupled into an optical fiber for delivery to the NPRO pump optics.

As described in more detail in the immediately preceding article, the output of each laser diode has a single-mode profile in the meridional plane containing an axis denoted the "fast" axis and a narrower multimode profile in the orthogonal meridional plane, which contains an axis denoted the "slow" axis. Also as before, one of the purposes served by the beam-combining optics is to reduce the fast-axis numerical aperture (NA) of the laser-diode output to match the NA of the optical fiber. Along the slow axis, the unmodified laser-diode NA is already well



Four Laser-Diode Beams are polarization-combined into two, then narrowed along the fast axis, then combined into one beam incident on an end face of an optical fiber.

matched to the fiber-optic NA, so no further slow-axis beam shaping is needed.

In this beam combiner (see figure), the laser-diode outputs are collimated by aspherical lenses, then half-wave plates and polarizing beam splitters are used to combine the four collimated beams into two beams. Spatial combination of the two beams and coupling into the optical fiber is effected by use of anamorphic prisms, mirrors, and a focusing lens. The anamorphic prisms are critical elements in the NA-matching scheme, in that they reduce

the fast-axis beam width to 1/6 of its original value. Inasmuch as no slow-axis beam shaping is needed, the collimating and focusing lenses are matched for 1:1 imaging. Because these lenses are well corrected for infinite conjugates, the combiner offers diffraction-limited performance along both the fast and slow axes.

This work was done by Paul Gelsinger and Duncan Liu of Caltech for NASA's Jet Propulsion Laboratory.

In accordance with Public Law 96-517, the contractor has elected to retain title to this

invention. Inquiries concerning rights for its commercial use should be addressed to:

*Innovative Technology Assets Management
JPL*

*Mail Stop 202-233
4800 Oak Grove Drive
Pasadena, CA 91109-8099
(818) 354-2240*

*E-mail: iaoffice@jpl.nasa.gov
Refer to NPO-43783, volume and number of this NASA Tech Briefs issue, and the page number.*

Spatial Combining of Laser-Diode Beams for Pumping an NPRO

Multiple multimode beams are efficiently combined into one optical fiber.

NASA's Jet Propulsion Laboratory, Pasadena, California

A free-space optical beam combiner now undergoing development makes it possible to use the outputs of multiple multimode laser diodes to pump a neodymium-doped yttrium aluminum garnet (Nd:YAG) non-planar ring oscillator (NPRO) laser while ensuring that the laser operates at only a single desired frequency. This optical beam combiner serves the same purpose as does the one described in "Diffractive Combiner of Single-Mode Pump Laser-Diode Beams" (NPO-42411), NASA Tech Briefs, Vol. 31, No. 5 (May 2007), page 16a. Although the principles of design and operation of the present and prior beam combiners are not identical, they are so closely related that it is necessary to devote the next four paragraphs to reiteration of a substantial portion of the cited prior article in order to give meaning to a description of the present beam combiner.

Heretofore, a Nd:YAG NPRO like the present one has been pumped by a single multimode laser-diode beam delivered via an optical fiber. It would be desirable to use multiple pump laser diodes to increase reliability beyond that obtainable from a single pump laser diode. However, as explained below, simplistically coupling multiple multimode laser-diode beams through a fiber-optic combiner would entail a significant reduction in coupling efficiency, and lasing would occur at one or more other frequencies in addition to the single desired frequency.

Figure 1 schematically illustrates the principle of operation of a laser-diode-pumped Nd:YAG NPRO. The laser beam path is confined in a Nd:YAG crystal by means of total internal reflections on

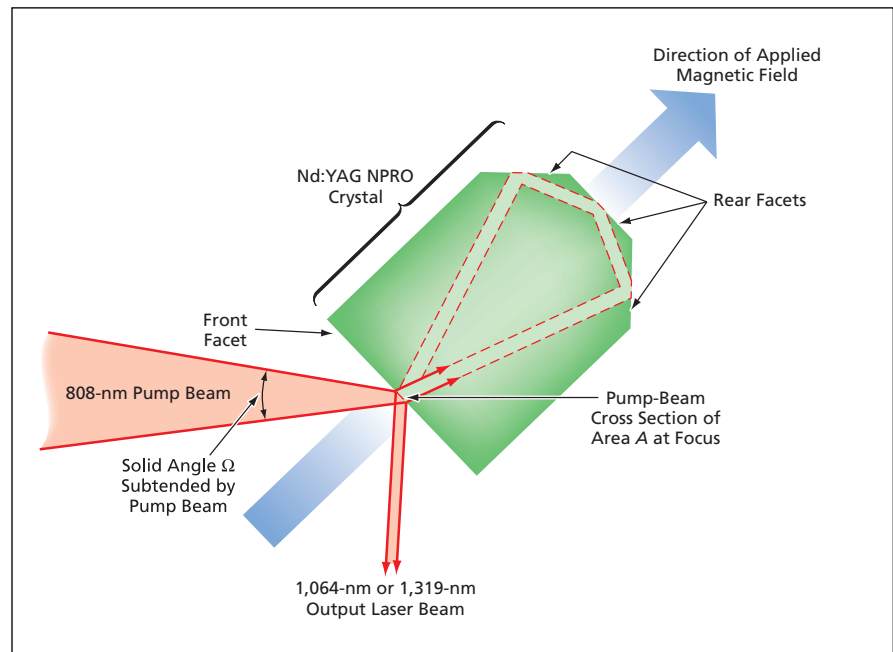


Figure 1. A Pump Beam of Solid Angle Ω has a cross section of area A at incidence upon the front facet of a Nd:YAG NPRO laser crystal.

the three back facets and an optical coating on the front facet. The wavelength of the pump beam — 808 nm — is the wavelength most strongly absorbed by the Nd:YAG crystal. The crystal can lase at a wavelength of either 1,064 nm or 1,319 nm — which one depending on the optical coating on the front facet.

In order to restrict lasing to a single frequency, it is necessary to confine the pump beam within the region occupied by the TEM_{00} mode of the NPRO laser beam near the front facet inside the crystal. In practice, this means that the pump beam must be focused to within a given solid angle (Ω) and area (A). [If a given

pump beam has a larger A or larger Ω but its $A\Omega$ is equal to or less than the maximum $A\Omega$ for single-frequency lasing in the crystal, then an imaging lens can be used to trade A against Ω so that both A and Ω are equal to or smaller than the maximum values for single-frequency lasing. It is possible to do this because it is a basic principle of optics that $A\Omega$ is preserved in imaging by a lens.]

The $A\Omega$ of a commercial multimode 808-nm laser diode of the type used heretofore is not axisymmetric; instead, it is elliptically distributed about the optical axis and, hence, does not match the circular distribution of a multimode

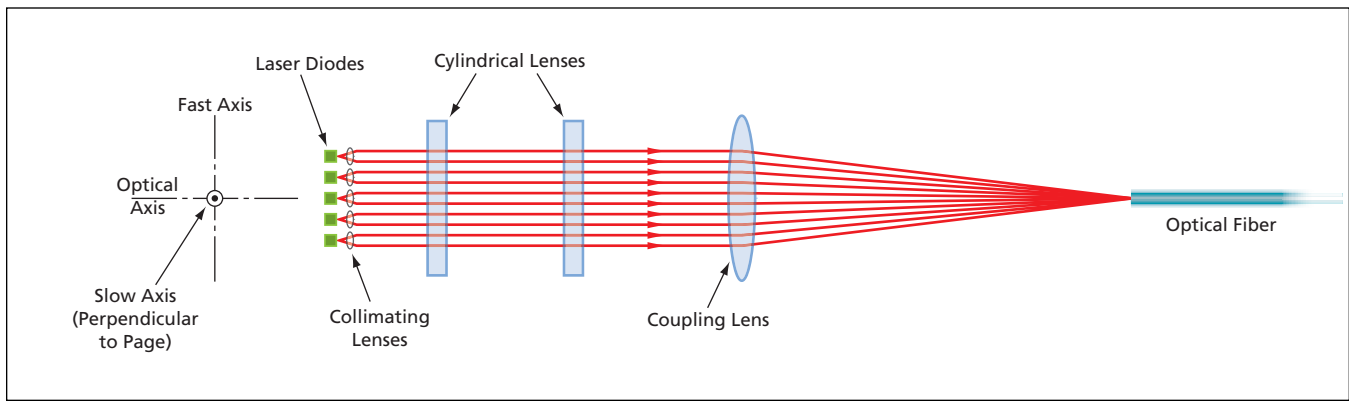


Figure 2. **Beams From Laser Diodes** stacked along the fast axis are focused onto the input face of an optical fiber by use of a combination of small collimating lenses and a larger lens here denoted the coupling lens. The cylindrical lenses cancel the magnifying effect of the collimating and coupling lenses in the slow-axis plane. This is a simplified and partly schematic view. In practice, it is necessary to position the laser diodes in a more complex layout and to use folding mirrors or prisms to direct beams along the optical axis of the coupling lens.

fiber of the type used heretofore to deliver a pump beam. As a result of this mismatch, $A\Omega$ for the pump beam emerging from the output end of the fiber is increased, typically to near the maximum single-frequency-lasing value in at least one of the planes containing the principal axes of the elliptical distribution. Consequently, it is difficult or impossible to maintain single-frequency lasing when combining the beams from two or more multimode laser diodes.

This concludes the reiteration of information from the cited prior article.

For a typical commercial 808-nm laser diode of the type upon which the design of the present beam combiner is based, the axes of the elliptical distribution are defined as follows: The far-field distribution of output optical power density is characterized by (1) a single-mode beam in a meridional plane containing an axis, perpendicular to the optical axis, that is customarily denoted the “fast” axis; and (2) a narrower multimode beam in the orthogonal meridional plane, wherein the axis perpendicular to the optical axis is customarily denoted the “slow.” The value

of $A\Omega$ in the fast-axis plane is only about 1/50 of that of the $A\Omega$ value associated with the combination of diameter (105 μm) and numerical aperture, NA, (0.15) of the optical fiber used to deliver the pump beam. Hence, it is possible to stack multiple laser diodes along the fast axis and couple their outputs into the same optical fiber, as shown in Figure 2.

To minimize coupling loss, one must ensure that the NA (≈ 0.3) of the combined laser-diode beams is less than the NA of the fiber. This amounts to a requirement to reduce the fast-axis NA of the beam from ≈ 0.3 to a value $< 0.15/N$ (where N is the number of laser-diode beams to be combined) and translates to a requirement to reduce the fast-axis divergence by use of a magnification factor of at least $0.3/(0.15/N) = 2N$. For example, a prototype to demonstrate this beam-combiner concept was designed using $N = 5$, for which required magnification factor is > 10 . In practice, to allow for alignment errors, a magnification factor of 19 was chosen for the prototype.

The $A\Omega$ of the laser-diode beam in the slow-axis plane is 1/1.3 as large as that of

the fiber. This $A\Omega$ is small enough to enable efficient coupling of light into the optical fiber, but too large for combining of beams in the slow-axis plane. Therefore, a pair of cylindrical lenses is used to cancel the slow-axis-plane magnification introduced by the non-cylindrical lenses used to effect magnification in the fast-axis plane.

This work was done by Paul Gelsinger, Duncan Liu, Jerry Mulder, and Francisco Aguayo of Caltech for NASA's Jet Propulsion Laboratory. Further information is contained in a TSP (see page 1).

In accordance with Public Law 96-517, the contractor has elected to retain title to this invention. Inquiries concerning rights for its commercial use should be addressed to:

*Innovative Technology Assets Management
JPL*

*Mail Stop 202-233
4800 Oak Grove Drive
Pasadena, CA 91109-8099
(818) 354-2240*

E-mail: iaoffice@jpl.nasa.gov

Refer to NPO-43782, volume and number of this NASA Tech Briefs issue, and the page number.



▶ Algorithm Optimally Orders Forward-Chaining Inference Rules

Requirements for exhaustive data-flow analysis are relaxed.

NASA's Jet Propulsion Laboratory, Pasadena, California

People typically develop knowledge bases in a somewhat *ad hoc* manner by incrementally adding rules with no specific organization. This often results in a very inefficient execution of those rules since they are so often order sensitive. This is relevant to tasks like Deep Space Network in that it allows the knowledge base to be incrementally developed and have it automatically ordered for efficiency.

Although data flow analysis was first developed for use in compilers for producing optimal code sequences, its usefulness is now recognized in many software systems including knowledge-based systems. However, this approach for ex-

haustively computing data-flow information cannot directly be applied to inference systems because of the ubiquitous execution of the rules. An algorithm is presented that efficiently performs a complete producer/consumer analysis for each antecedent and consequence clause in a knowledge base to optimally order the rules to minimize inference cycles.

An algorithm was developed that optimally orders a knowledge base composed of forwarding chaining inference rules such that independent inference cycle executions are minimized, thus, resulting in significantly faster execution. This algorithm was integrated into the

JPL tool Spacecraft Health Inference Engine (SHINE) for verification and it resulted in a significant reduction in inference cycles for what was previously considered an ordered knowledge base. For a knowledge base that is completely unordered, then the improvement is much greater.

This work was done by Mark James of Caltech for NASA's Jet Propulsion Laboratory. Further information is contained in a TSP (see page 1).

The software used in this innovation is available for commercial licensing. Please contact Karina Edmonds of the California Institute of Technology at (626) 395-2322. Refer to NPO-42003.

▶ Project Integration Architecture

All information of technological processes can be readily originated, manipulated, shared, propagated to other processes, and viewed by man or machine.

John H. Glenn Research Center, Cleveland, Ohio

The Project Integration Architecture (PIA) is a distributed, object-oriented, conceptual, software framework for the generation, organization, publication, integration, and consumption of all information involved in any complex technological process in a manner that is intelligible to both computers and humans. As used here, "all information" signifies, more specifically, all information that has been or could be coded in digital form. This includes not only experimental data, design data, results of simulations and analyses, organizational and financial data, and the like, but also sets of rules, computer programs, processes, and methods of solution.

In the development of PIA, it was recognized that in order to provide a single computational environment in which all information associated with any given complex technological process could be viewed, reviewed, manipulated, and shared, it is necessary to formulate all the elements of such a process on the most fundamental level. In this formulation, any such element is regarded as being composed of any or all of

three parts: input information, some transformation of that input information, and some useful output information.

Another fundamental principle of PIA is the assumption that no consumer of information, whether human or computer, can be assumed to have any useful foreknowledge of an element presented to it. Consequently, a PIA-compliant computing system is required to be ready to respond to any questions, posed by the consumer, concerning the nature of the proffered element. In colloquial terms, a PIA-compliant system must be prepared to provide all the information needed to place the element in context.

To satisfy this requirement, PIA extends the previously established object-oriented-programming concept of self-revelation and applies it on a grand scale. To enable pervasive use of self-revelation, PIA exploits another previously established object-oriented-programming concept — that of semantic infusion through class derivation. By means of self-revelation and semantic

infusion through class derivation, a consumer of information can inquire about the contents of all information entities (e.g., databases and software) and can interact appropriately with those entities.

Other key features of PIA include the following:

- Encapsulation of dimensionality and other semantically appropriate functionality;
- Enforcement of the dimensional nature of information (that is, something that is dimensional in nature cannot be accessed in a dimensionally-unaware manner);
- Exploitation of the object-identification facilities of the Common Object Request Broker Architecture (CORBA) to provide an object "address space" (defining the quantity of information that can be stored) that reaches to a practical infinity;
- Use of the object-etherealization and -incarnation facilities of the CORBA to make feasible the serving of a practically infinite number of objects;

- Use of file-system directory structures to make organization of, and access to, files reaching to a practical infinity feasible and efficient;
 - Provision of facilities to enable the storage of object state files in multiple locations, including locations accessible on the Internet through CORBA communication capabilities;
 - Provision of a distributed, lock-management system to efficiently provide for resolution of concurrent-access issues and, at the appropriate level, to apply per-user, per-object access controls;
 - Provision of a flexible event system so that attention or help can be automatically summoned when significant situations occur, significant information is found, and the like; and
 - Use of encryption to secure the transport of information when desired.
- The key benefits afforded by PIA include the following:
- Such software tools as graphical user interfaces, browsers, and search engines can be used to identify, view, manipulate, and share information from a practically unlimited number of resources;
 - Information can flow seamlessly and inerrantly between application pro-

- grams and other information resources participating in the coordinated solution of a large problem;
- Because PIA is not discipline-specific, disparate technologies and their organizations can interoperate seamlessly when such needs arise;
 - Flexibility in the integration of application programs is increased by enabling their authors to focus on the kinds of information needed rather than on the sources of the information;
 - The identification of information propagation paths in integrated analyses is done by the machine, rather than by a person, thus reducing or eliminating the variability and occasional inaccuracy of human-directed efforts;
 - Entire explorations of significant, planet-level technological problems can be captured and retained in an auditable, verifiable manner;
 - The inherent parallelism of sibling activities is exploited to enable the concurrent investigation and analysis of planet-level technological problems by a practically infinite host of computers;
 - PIA provides facilities by means of which it might become possible to automatically devise a method of solution of significant, planet-level technological problems and both the process of devis-

ing the method of solution and the method of solution itself could become a part of the body of available information;

- The potential ability to automatically devise methods of solution offers the possibility of developing adaptive, resilient systems that can “heal themselves” when individual elements fail or become unavailable;
- By providing such a mass of information in a single, cohesive environment, the automated search for recurrent patterns, themes, and the like is enabled; and
- PIA offers the potential for a new form of software product delivery in which the services of a software product are provided through a PIA-compliant server while the software, itself, remains closely held and managed by its owner.

This work was done by William Henry Jones of Glenn Research Center. Further information is contained in a TSP (see page 1).

Inquiries concerning rights for the commercial use of this invention should be addressed to NASA Glenn Research Center, Innovative Partnerships Office, Attn: Steve Fedor, Mail Stop 4-8, 21000 Brookpark Road, Cleveland, Ohio 44135. Refer to LEW-17961-1.



Books & Reports

High Power Amplifier and Power Supply

A document discusses the creation of a high-voltage power supply (HVPS) that is able to contain voltages up to -20 kV, keep electrical field strengths to below 200 V/mil (≈ 7.87 kV/mm), and can provide a 200-nanosecond rise/fall time focus modulator swinging between cathode potential of 16.3 kV and -19.3 kV. This HVPS can protect the 95-GHz, pulsed extended interaction klystron (EIK) from arcs/discharges from all sources, including those from within the EIK's vacuum envelope.

This innovation has a multi-winding pulse transformer design, which uses new winding techniques to provide the same delays and rise/fall times (less than 10 nanoseconds) at different potential levels ranging from -20 kV to -16 kV. Another feature involves a high-voltage printed-wiring board that was corona-free at -20 kV DC with a 3-kV AC swing. The corona-free multi-layer high-voltage board is used to simulate fields of less than 200 V/mil (≈ 7.87 kV/mm) at 20 kV DC. Drive techniques for the modulator FETs (field-effect transistors) (four to 10 in a series) were created to change states (3,000-V swing) without abrupt steps, while still maintaining required delays and transition times. The packing scheme includes a potting mold to house a ten-stage modulator in the space that, in the past, only housed a four-stage modulator.

Problems keeping heat down were solved using aluminum oxide substrate in the high-voltage section to limit temperature rise to less than 10° while withstanding -20 kV DC voltage and remaining corona-free.

This work was done by Johnny Duong, Scot Stride, Wayne Harvey, Inam Haque, Newton Packard, Quintin Ng, and Julie Y. Ispirian of Caltech; Christopher Waian of Robert M. Hadley Co.; and Drew Janes of Vallet Syncom Circuits for NASA's Jet Propulsion Laboratory. Further information is contained in a TSP (see page 1).

In accordance with Public Law 96-517, the contractor has elected to retain title to this

invention. Inquiries concerning rights for its commercial use should be addressed to:

Innovative Technology Assets Management, JPL, Mail Stop 202-233, 4800 Oak Grove Drive, Pasadena, CA 91109-8099, (818) 354-2240, E-mail: iaoffice@jpl.nasa.gov.

Refer to NPO-44241, volume and number of this NASA Tech Briefs issue, and the page number.

Estimating Mixing Heights Using Microwave Temperature Profiler

A paper describes the Microwave Temperature Profiler (MTP) for making measurements of the planetary boundary layer thermal structure — data necessary for air quality forecasting as the Mixing Layer (ML) height determines the volume in which daytime pollution is primarily concentrated. This is the first time that an airborne temperature profiler has been used to measure the mixing layer height. Normally, this is done using a radar wind profiler, which is both noisy and large.

The MTP was deployed during the Texas 2000 Air Quality Study (TexAQS-2000). An objective technique was developed and tested for estimating the ML height from the MTP vertical temperature profiles. In order to calibrate the technique and evaluate the usefulness of this approach, estimates from a variety of measurements during the TexAQS-2000 were compared. Estimates of ML height were used from radiosondes, radar wind profilers, an aerosol backscatter lidar, and *in-situ* aircraft measurements in addition to those from the MTP.

Relative to the benchmark radiosonde estimates, radar wind profiler ML height estimates were nearly bias-free. Airborne lidar and profiler estimates generally were in good agreement inland, but spatial gradients of ML heights made comparisons difficult near the coast. The presence of a residual layer above the sea breeze was probably responsible for a gross overestimate of ML height by lidar in a few instances. The accuracy of the MTP-based ML height estimates is similar to that of other techniques for estimating ML height. The airborne MTP thus shows

promise for measuring the spatial distribution of ML structure, especially in coastal environments where aerosol lidars may have difficulty identifying the ML.

This work was done by John Nielson-Gammon and Christina Powell of Texas A&M University; Michael Mahoney of Caltech; and Wayne Angevine of CIRES for NASA's Jet Propulsion Laboratory. For more information, contact iaoffice@jpl.nasa.gov. NPO-43887

Multiple-Cone Sunshade for a Spaceborne Telescope

A document describes a sunshade assembly for the spaceborne telescope of the Terrestrial Planet Finder Coronagraph mission. During operation, the telescope is aimed at target stars in the semi-hemisphere away from the Earth's Sun. The observatory rotates about its pointing axis during a single star observation, resulting in relative movement of the Sun. The sunshade assembly protects the telescope against excessive solar-induced thermal distortions for times long enough to complete observations.

The assembly includes a cylindrical baffle immediately surrounding the telescope, and a series of coaxial conical shields at half-cone angle increments of between 3° and 6° . The black inner surface of the cylindrical baffle suppresses stray light. The outer surface of the cylindrical baffle and all the surfaces of the conical shields except the outermost one are specular and highly reflective in the infrared. The outer surface of the outer shield is a material with low solar absorptance and high infrared emittance, such as silverized Teflon or white paint. This arrangement strongly radiatively couples each shield layer more effectively to cold space than to adjacent shield layers. The result is that the solar-driven temperature gradients in the cylindrical baffle are nearly negated, and only weakly communicated to the highly-infrared-reflective face of the primary telescope mirror.

This work was done by Terry Cafferty of TC Technology and Virginia Ford of Caltech for NASA's Jet Propulsion Laboratory. Further information is contained in a TSP (see page 1). NPO-41419



National Aeronautics and
Space Administration